

1 **Urban-rural patterns and driving factors of particulate 2 matter pollution decrease in eastern china**

3 Zhihao Song^{1, 2}, Bin Chen^{1, 2*}

4 ¹ College of Atmospheric Sciences, Lanzhou University, Lanzhou 730000, China

5 ² Institute of Meteorological Artificial Intelligence Research, Lanzhou University, Lanzhou 730000, China

6 *Correspondence to:* Bin Chen (chenbin@lzu.edu.cn)

7 **Abstract.** Understanding the urban-rural patterns and driving drivers behind the recent decrease in
8 particulate matter (PM) pollution across eastern China is essential for assessing the efficacy of
9 environmental policies and ensuring equitable health co-benefits. By employing an interpretable, end-
10 to-end machine learning framework integrating satellite observations, meteorological factors, and
11 auxiliary datasets, this study reveals changes in urban and rural PM pollution and the underlying drivers.

12 During the period 2015-2023, the average decrease rates of PM₁₀ and PM_{2.5} in eastern China were -
13 $4.02 \pm 1.29 \mu\text{g}/\text{m}^3/\text{yr}$ and $-2.41 \pm 0.91 \mu\text{g}/\text{m}^3/\text{yr}$, respectively. The rate of decrease in urban areas was higher
14 than that in rural areas, which played a dominant role in PM reduction. Significant reductions in PM
15 concentrations were observed in urban core areas, suburbs, towns and regions with high agricultural
16 pressure. The interpretability analysis showed that temperature and interannual variability were the main
17 drivers of PM pollution reduction. However, only interannual variability showed a significant decreasing
18 trend in its effect on PM pollution, while other driving factors showed periodic variations. Furthermore,
19 there were differences in the drivers of PM reduction between urban and rural areas, particularly with
20 interannual variability in particular contributing to PM pollution reduction in urban areas, but having a
21 lesser impact in most rural areas. This study reveals the urban-rural patterns of PM pollution reduction
22 in eastern China, and highlights the need for differentiated air pollution control strategies in urban and
23 rural areas.

24 **1 Introduction**

25 Air pollution caused by PM_{2.5} and PM₁₀ (airborne particulate matter with diameters less than 2.5 μm
26 and 10 μm , respectively) has adversely affected China's atmospheric environment (Huang et al., 2014a;
27 Zhang et al., 2012). PM pollution is now considered the greatest environmental risk factor for global

28 human health (Apte et al., 2015), as exposure to PM can trigger various respiratory and cardiovascular
29 diseases (Burnett Richard et al., 2014; West et al., 2016; Cohen et al., 2017). The indirect health risks
30 associated with PM exposure (Yin et al., 2020) contribute to millions of premature deaths annually in
31 China (Burnett et al., 2018). To mitigate the escalating risks of particulate matter exposure and reduce
32 the public health burden, the Chinese government introduced the "Air Pollution Prevention and Control
33 Action Plan" in 2013 (State Council of the People's Republic of China, 2013). This initiative aims to
34 implement policies to improve energy efficiency, reduce energy-related pollution, and curb
35 anthropogenic emissions to control particulate matter pollution in the atmosphere (State Council of the
36 People's Republic of China, 2014). As a result of this initiative, China's atmospheric particulate matter
37 pollution has improved significantly (Cheng et al., 2021). Between 2013 and 2017, the annual average
38 concentration of $PM_{2.5}$ decreased by 28-40% (Zheng et al., 2018; Ministry of Ecology and Environment
39 of the People's Republic of China, 2017), and the population-weighted national annual average
40 concentration of $PM_{2.5}$ decreased by 32% (Xue et al., 2019). Data from the National Air Quality
41 Monitoring Network show that between 2013 and 2020, the annual average $PM_{2.5}$ concentration in urban
42 areas of China decreased from $72 \mu\text{g}/\text{m}^3$ to $33 \mu\text{g}/\text{m}^3$ (Song et al., 2023). As a result, the Clean Air Action
43 has achieved remarkable results in reducing PM pollution (Zhang et al., 2019b).

44 It is widely accepted that improvements in air quality can be attributed to both reductions in
45 anthropogenic emissions (Geng et al., 2019; Zheng et al., 2023; Zhao et al., 2018) and changes in
46 meteorological conditions (An et al., 2019; Cao and Yin, 2020; Chen et al., 2020a). To assess the driving
47 factors behind changes in PM concentration trends, it is essential to distinguish between anthropogenic
48 emissions and meteorological factors (Zhong et al., 2018). Zhong et al. (2021) found that $PM_{2.5}$
49 concentrations decreased by 44% from 2013 to 2019, and by 34% when the influence of meteorological
50 conditions was excluded, thus demonstrating the effectiveness of emission reduction measures. Qiu et al.
51 (2022) used the GEOS-Chem chemical transport model to simulate the impact of anthropogenic
52 emissions on PM pollution trends and provided recommendations for attributing PM pollution trends to
53 emission changes. Vu et al. (2019) used machine learning to assess the impact of air quality trends in
54 Beijing and found that $PM_{2.5}$ and PM_{10} concentrations decreased by 34% and 24%, respectively, after
55 excluding meteorological influences, attributing the decrease to reduced coal burning. Zhai et al. (2019)
56 used a stepwise multiple linear regression (MLR) model to quantify $PM_{2.5}$ trends in China between 2013

57 and 2018, and found that meteorological conditions contributed about 12%. However, Xiao et al. (2021)
58 used statistical methods to separate the contributions of emissions and meteorology to long-term PM_{2.5}
59 trends in East China, and found that meteorological contributions were even higher in certain years.
60 Overall, distinguishing the contributions of anthropogenic emissions and meteorological changes to PM
61 pollution is crucial to improve understanding of pollution processes and to inform pollution control
62 policies and future air quality predictions.

63 However, the urban-rural patterns of PM pollution improvement remain poorly understood in
64 existing research (Chen et al., 2020b). Many studies on PM pollution either focus on highly polluted
65 regions (such as the Beijing-Tianjin-Hebei region) (Chen et al., 2019b; Chen et al., 2019c), or on
66 developed regions with a high concentration of large cities (such as the Yangtze River Delta and the
67 Pearl River Delta) (Gui et al., 2019; He et al., 2017). This focus is mainly due to the high concentrations
68 of air pollutants in developed cities (Sicard et al., 2023), where PM pollution poses a significant public
69 health threat to densely populated urban areas (Brauer et al., 2016; Southerland et al., 2022). Although
70 PM pollution in urban areas highlights the importance of environmental governance, rural areas, with
71 different consumption habits and living conditions (e.g., solid fuel burning in households) (Li et al.,
72 2014)), may experience air pollution that differs from urban areas (Wang et al., 2024a). In certain seasons
73 and regions, PM exposure factors in rural areas are generally higher than those in urban areas, with
74 exposure levels reaching up to 70% (Wang et al., 2024b). Therefore, the contribution of these regions to
75 PM pollution improvement may differ (Li et al., 2024b). Without targeted assessments, perceptions of
76 the relative importance of urban and rural areas in China's air pollution control efforts may be distorted,
77 hindering the development of appropriate environmental policies and the promotion of green
78 development in urban and rural construction (Yang et al., 2024).

79 Currently, many studies have used machine learning models to obtain particulate matter
80 concentration products and apply them to pollution assessment (Chen et al., 2019a; Huang et al., 2021).
81 Among these, extreme tree models and data from the Himawari-8 satellite have demonstrated outstanding
82 performance (Wei et al., 2021b; Wei et al., 2021a; Wei et al., 2021c). In particular, the extreme tree
83 model demonstrates its unique advantages, including greater randomness and interference resistance, and
84 outperforms other similar models in terms of performance (Wei et al., 2023). This study advances the
85 understanding of the current status and driving factors of urban-rural PM pollution improvement using

86 interpretable machine learning methods. First, by integrating Himawari-8/9 satellite top-of-atmosphere
87 reflectance (TOAR) data, meteorological data, and geographic information, we use a multiple-output
88 extreme trees (MOET) model to capture the spatiotemporal distribution of PM (including PM₁₀ and PM_{2.5})
89 across China and assess the patterns of PM pollution improvement. We then use various machine learning
90 interpretability techniques, such as relative importance, tree interpreters, and SHAP values, to quantify
91 the contributions of anthropogenic emissions and meteorological changes to PM pollution improvement.
92 To investigate potential differences in the results between urban and rural areas, we use land use data to
93 distinguish urban from rural regions in eastern China. This study aims to address the following three
94 questions: (1) What are the spatio-temporal patterns of PM pollution improvement in urban and rural
95 areas of China? (2) What are the main driving factors behind the differences in PM pollution
96 improvement between urban and rural areas? (3) What are the specific contributions of each driving
97 factor to PM pollution improvement? Answering these questions is crucial for a comprehensive
98 understanding of the dynamics of urban and rural atmospheric particulate pollution control in China.

99 **2 Data and Methods**

100 **2.1 Satellite TOAR data and ground-based PM observations**

101 Previous studies have shown that satellite-observed top-of-atmosphere reflectance (TOAR) data
102 can be used to estimate near-surface air pollutants (Chen et al., 2024a; Yang et al., 2023; Song et al.,
103 2024). In particular, the TOAR data from the Himawari-8 satellite have demonstrated excellent
104 performance in pollutant estimation (Hu et al., 2022; Liu et al., 2019). The Advanced Himawari Imager
105 (AHI) on board the Himawari-8/9 satellite is an advanced passive observation instrument with 16
106 observation channels, providing a spatiotemporal resolution of up to 10 minutes and 0.5 km (Bessho et
107 al., 2016). Based on the sensitivity of the AHI sensor (Yoshida et al., 2018), three visible channels (0.46
108 μm , 0.51 μm , and 0.64 μm) and two near-infrared channels (0.86 μm and 2.3 μm) were used in this study.
109 In addition, four angles related to aerosol inversion results: SAA (satellite azimuth angle), SAZ (satellite
110 zenith angle), SOA (solar azimuth angle), and SOZ (solar zenith angle) were also included in the study.
111 TOAR data from the AHI imager were obtained from the Himawari Monitor P-Tree System data
112 download website of the Japan Meteorological Agency (<https://www.eorc.jaxa.jp/ptree/index.html>). The

113 time range for Himawari-8 data is from September 1, 2015, to September 30, 2022, while the time range
114 for Himawari-9 data is from October 1, 2022, to August 31, 2023.

115 The ground-based PM data were provided by the China National Environmental Monitoring Center
116 (CNEMC) (<http://www.cnemc.cn>) and were calibrated and quality controlled according to the Chinese
117 National Standard GB 3095-2012 (Ministry of Ecology and Environment of the People's Republic of
118 China, 2012). In this study, hourly mean PM_{10} and $PM_{2.5}$ data were collected from approximately 1,400
119 stations in eastern China (102-136°E, 16-56°N) for the period from 1 September 2015 to 31 August 2023.
120 Observations with $PM_{2.5}$ concentrations above 600 $\mu\text{g}/\text{m}^3$ or PM_{10} concentrations above 1,000 $\mu\text{g}/\text{m}^3$, as
121 well as those with concentrations below 1 $\mu\text{g}/\text{m}^3$, were excluded (Shi et al., 2024).

122 **2.2 Meteorological data and geographic information data**

123 Studies assessing the impact of meteorological factors on PM pollution have identified temperature,
124 humidity, and wind as the main variables influencing $PM_{2.5}$ concentrations, with their effects
125 significantly outweighing those of other factors. Among these, temperature has the most significant
126 and stable influence (Chen et al., 2018b). In this study, meteorological data were obtained from
127 the ERA-5 reanalysis dataset provided by the European Centre for Medium-Range Weather Forecasts
128 (<https://cds.climate.copernicus.eu/cdsapp#!/dataset/>). The dataset includes boundary layer height
129 (BLH), relative humidity (RH), surface pressure (SP), 2-metre air temperature (T2M), wind direction
130 (WD), wind speed (WS), and net solar radiation at the surface (NSR), with spatial resolutions
131 of $0.1^\circ \times 0.1^\circ$ or $0.25^\circ \times 0.25^\circ$ (Hersbach et al., 2020). Geographic information can also influence
132 pollutant concentrations to some extent due to variations in meteorological conditions (Chen
133 et al., 2018a; Chen et al., 2021). The geographic information data used in this study include elevation
134 (HEIGHT), land cover type (LUCC), and population density (RK). HEIGHT is derived from
135 SRTM-3 elevation data, with a spatial resolution of 90 meters and a temporal resolution of 1 year.
136 The download URL is <https://doi.org/10.5067/MEaSURES/SRTM/SRTMGL3.003>. LUCC is sourced
137 from the dataset (MCD12Q1), with a spatial resolution of 500 meters and a temporal resolution
138 of 1 year. The download URL is <https://doi.org/10.5067/MODIS/MCD12Q1.006>, used to describe
139 land surface types and land use conditions. RK is derived from the 2015 United Nations adjusted
140 population density data, with a spatial resolution of $0.1^\circ \times 0.1^\circ$ and a temporal resolution of 1 year,
141 available at <https://doi.org/10.7927/H4PN93PB>. It is provided by the Social and Economic Data

142 and Applications Center (SEDAC) of the National Aeronautics and Space Administration (NAS
143 A).

144 **2.3 Data integration and development of the Multiple-Output Extreme Trees Model**

145 The resolution of the meteorological and geographic information data was adjusted to $0.05^\circ \times 0.05^\circ$
146 using bilinear interpolation. All data were then matched with station data according to the $0.05^\circ \times 0.05^\circ$
147 grid of the Himawari-8 satellite. The specific matching method is described in detail in Chen et al. (2022c)
148 and Song et al. (2022b).

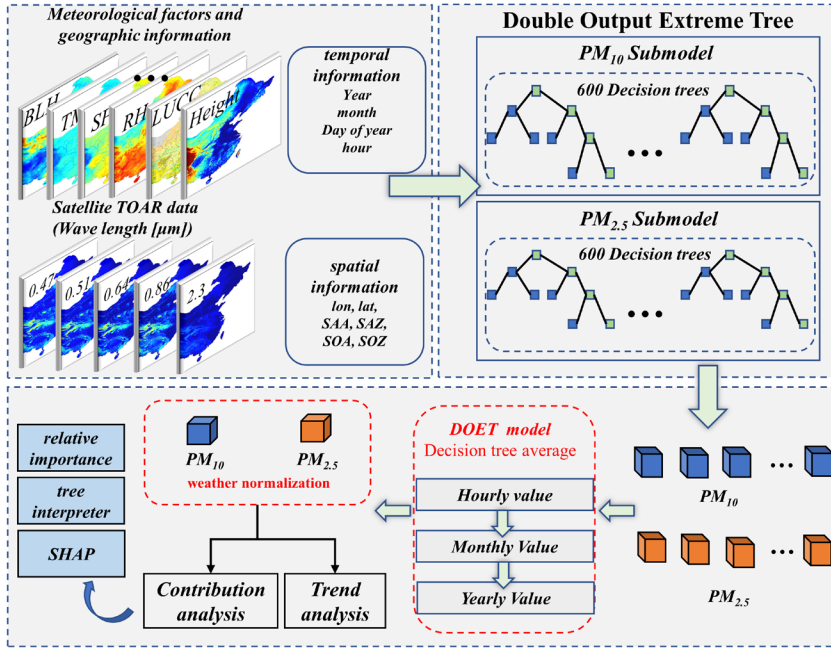
149 The DOET model is developed on the basis of the Extreme Trees (ET) model (Geurts et al., 2006),
150 which is capable of simultaneously handle multi-target variable output tasks. The ET model is similar to
151 the Random Forest (RF) model, both of which consist of multiple decision trees. However, whereas the
152 RF model randomly samples data with replacement, the ET model uses all available samples. After
153 determining the samples and features, the ET model constructs decision trees based on optimal partition
154 attributes. This process is repeated until a sufficient number of decision trees have been constructed to
155 form the ET model. Finally, the average regression results of all decision trees in the ET are used as the
156 final output. Several studies have confirmed that the ET model has excellent fitting performance (Qin et
157 al., 2020; Zhang et al., 2022a; Chen et al., 2022a).

158 In this study, three model parameters were optimized: the number of trees (n_estimators), the
159 maximum depth of the model (max_depth), and the minimum number of samples required to split a node
160 (min_samples_split). After balancing the accuracy and efficiency of the model, these parameters were
161 set to 70, 100, and 5, respectively. The model, which uses satellite observations, meteorological data,
162 and geographical information to estimate near-surface PM concentrations, can be expressed as:

$$163 (PM_{10}, PM_{2.5}) = f \left(\begin{array}{l} TOAR_{1,2,3,4,6}, BLH, RH, SP, T2M, WD, WS, NSR, Height, LUCC, RK, \\ year, mon, doy, hour, lon, lat, SAA, SAZ, SOA, SOZ \end{array} \right) \quad (1)$$

164 Here, f represents the DOET model, and $TOAR_{1,2,3,4,6}$ denotes the radiance values of the three
165 visible channels (0.46 μm , 0.51 μm , and 0.64 μm) and the two near-infrared channels (0.86 μm and 2.3
166 μm). $BLH, RH, SP, T2M, WD, WS$ and NSR are meteorological variables, while $Height, LUCC$ and
167 RK represent geographical information. The variables lon (Longitude), lat (Latitude), SAA , SAZ , SOA
168 and SOZ representing spatial information. The variables $year$, mon (month), doy (day of the year), and
169 $hour$ are temporal information reflecting the influence of anthropogenic emissions on PM pollution (Wei

170 et al., 2020). Time variables (year, month) effectively characterize cyclical patterns and long-term trends
171 in human activity, serving as reliable proxy indicators in pollution analysis (Song et al., 2023). Monthly
172 cycles directly reflect seasonal rhythms: winter heating spikes PM2.5 and SO₂ levels (Liu et al., 2017),
173 agricultural phases amplify ammonia emissions (Ma et al., 2025), and transportation peaks during
174 holidays elevate NO₂ concentrations (Hua et al., 2021). Annual trends capture industrial evolution and
175 policy impacts, such as the PM2.5 reduction after implementing the "Air Pollution Prevention Action
176 Plan" (Geng et al., 2024; Geng et al., 2021). As standardized, quantifiable metrics, time variables
177 circumvent data limitations for complex activities (e.g., energy consumption, economic behaviors, urban
178 sprawl), enable cross-regional comparisons without normalization, and reveal pollution responses to
179 socioeconomic rhythms and policy efficacy (Dai et al., 2021; Shi et al., 2021). Specifically, year and
180 month (mon) are used to represent the interannual and intra-annual variations in anthropogenic emissions,
181 respectively (Zhang et al., 2019a; Park et al., 2019). The estimation workflow is illustrated in Figure 1.
182 The specific estimation process of the DOET model is as follows: firstly, meteorological factors,
183 geographic information, and satellite TOAR data are input into the DOET model and matched with PM
184 observation data. Then, the DOET model fits the PM observation data with the input variables to obtain
185 two ET estimation models (PM₁₀ and PM_{2.5}). Finally, the two ET models are integrated to obtain the
186 DOET model, and the estimation results of PM₁₀ and PM_{2.5} are output simultaneously to save
187 computation time. Finally, the obtained PM₁₀ and PM_{2.5} data are subjected to further analysis.
188 Additionally, we performed weather normalization on the PM data to mitigate the impact of
189 meteorological events (Grange and Carslaw, 2019).



190
191 **Figure 1. Workflow of PM data estimation and pollution driving factors assessment.**

192 Model performance was evaluated using 10-fold cross-validation (Rodriguez et al., 2010),
193 incorporating sample-based, space-based, and time-based validation methods (Wei et al., 2019).
194 Evaluation metrics used included the coefficient of determination (R^2), root mean square error (RMSE),
195 and mean absolute error (MAE) for both PM_{10} and $PM_{2.5}$ (Chen et al., 2023).

196
$$R^2 = 1 - \frac{ss_{res}}{ss_{tot}} \quad (2)$$

197
$$MAE = \frac{1}{n} \sum_{i=1}^n |\hat{y}_i - y_i| \quad (3)$$

198
$$RMSE = \sqrt{\frac{1}{n} \sum_{i=1}^n (\hat{y}_i - y_i)^2} \quad (4)$$

199 In Equation (2), ss_{res} represents the error between the estimated value of the model and the
200 average value of the observed values of PM_{10} and $PM_{2.5}$, ss_{tot} represents the error between the observed
201 values of PM_{10} and $PM_{2.5}$ and the average value of the observed values of PM_{10} and $PM_{2.5}$ from CNEMC.
202 In Equation (3-5), \hat{y}_i represents the PM_{10} and $PM_{2.5}$ estimated value of the DOET model, y_i represents
203 the observed value of PM_{10} and $PM_{2.5}$ from CNEMC.

204 **2.4 Machine learning interpretability variables**

205 To investigate the influence of potential driving factors on PM pollution improvement in eastern
206 China, we employed relative importance (Berner et al., 2020), tree interpreter (Wang et al., 2022b), and

207 SHapley Additive exPlanations (SHAP) (Lundberg and Lee, 2017) to distinguish the contributions of
208 meteorological changes and anthropogenic emissions to PM pollution improvement. Relative importance
209 was assessed using the permutation importance value of the DOET model, defined as the average
210 reduction in model accuracy when a single feature value is randomly shuffled (Yang et al., 2022).

211 The permutation importance of each variable was calculated using the “permutation_importance”
212 library in Python. To reduce uncertainty, the training process was repeated 20 times for each grid point
213 to obtain robust estimates of relative importance (Qu et al., 2023). The tree interpreter was applied using
214 the 'tree_interp_functions' library in Python, which is designed for predictions based on decision tree
215 ensemble models and facilitates the decomposition of each prediction into bias and feature contribution
216 components. The detailed calculation method and code for the tree interpreter can be obtained from the
217 following URL:<https://github.com/andosa/treeinterpreter/tree/master>.

218 SHAP values are based on Shapley value theory, which explains model predictions by calculating
219 the relative contribution of each feature to the output (He et al., 2024). These values reflect not only the
220 influence of features on individual samples but also indicate the positive and negative contributions of
221 these influences. SHAP explanations can be applied to any machine learning model, including neural
222 networks and ensemble models, and provide comprehensive and accurate interpretability results. Thus,
223 the SHAP method provides superior explanations for both local and global model effects (Liu et al., 2023;
224 Hou et al., 2022). In Python, “tree_SHAP” is specifically tailored for decision tree-based machine
225 learning models, such as the Extreme Tree model, to provide greater accuracy and faster computation.

226 The interpretability variables described above were applied to the monthly averaged PM₁₀ and PM_{2.5}
227 datasets generated by the DOET model.

228 **2.5 Land cover type classification**

229 Zhang et al. (2022b) proposed a method to differentiate urban and rural areas based on the gradient
230 of human land use pressure. In this study, the MCD12Q1 land cover map, with a spatial resolution of 500
231 meters was used. For grids measuring 5×5 km, urban and rural classifications were determined by the
232 coverage of specific land cover categories (e.g., urban land and cropland), which reflect the transition
233 from urban to rural areas and correspond to different levels of human activity. As shown in Table 1 and
234 Figure S1, urban areas in this study include both urban core areas and suburban regions, while rural areas
235 are categorized into six types: towns, high agricultural pressure areas, low agricultural pressure areas,

236 forests and grasslands.

237 **Table 1. Definitions of urban and rural land cover classes**

Urban-Rural Land Cover Class	Definition
Urban	50%<Urban grid
Suburban	25%<Urban grid<50%
Towns	12.5%<Urban grid<25%
High Agricultural Pressure Areas	50%<Cropland grid
Low Agricultural Pressure Areas	12.5%< Cropland grid grid<50%
Forests	50%<Forest grid
Grasslands	50%<Grassland grid
Other	Remaining unclassified grids (e.g., desert or tundra)

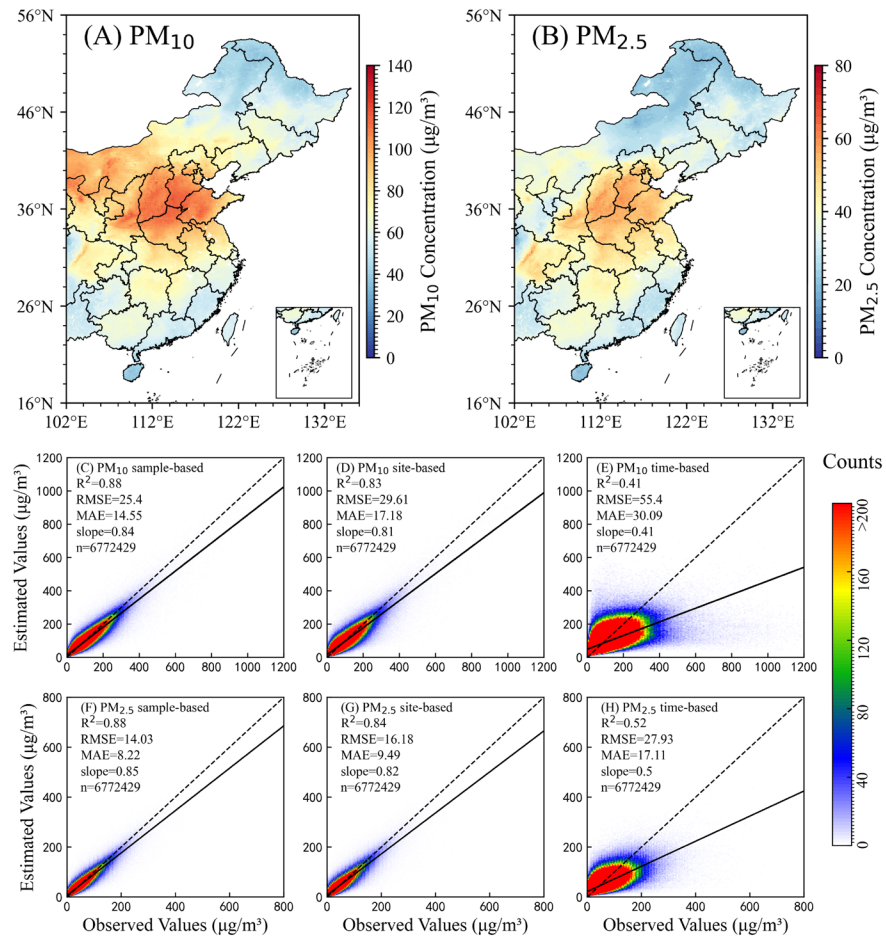
238 **3 Results**

239 **3.1 PM estimation model performance and PM distribution characteristics**

240 For the period from September 2015 to August 2023 in eastern China, a total of 6,772,429 samples
241 were matched. After parameter optimization and feature training, the optimal DOET model was derived,
242 and long-term time-series spatial distribution products for PM_{10} and $PM_{2.5}$ in eastern China were
243 generated. Figure 2 shows the results of 10-fold cross-validation based on sample, spatial and temporal
244 validations. Overall, the DOET model showed a high level of accuracy in the estimation of PM data. The
245 sample-based 10-fold cross-validation results (Figure 2C and 2F) yielded an R^2 of 0.87, with RMSE
246 (MAE) values of 25.82 (14.87) $\mu\text{g}/\text{m}^3$ for PM_{10} and 14.36 (8.44) $\mu\text{g}/\text{m}^3$ for $PM_{2.5}$. The slope of the fitting
247 line between observed and estimated values was 0.84. The performance of the DOET model in this study
248 is comparable to that reported in other studies that estimated PM using Himawari-8 TOAR data (Wang
249 et al., 2021; Chen et al., 2024b; Yin et al., 2021).

250 The 10-fold cross-validation results based on spatial and temporal validation were slightly lower
251 than those based on samples (Figures 2D-E and 2G-H). Spatial validation assessed the performance of
252 the model in estimating PM concentrations in areas without monitoring stations, after training the model
253 with samples from areas with stations. Temporal validation involved training the model with samples
254 from specific years and testing it with data from years not used in training. For these two validation
255 methods, the R^2 values for PM_{10} were 0.83 and 0.41, with RMSE values of 29.99 $\mu\text{g}/\text{m}^3$ and 55.44 $\mu\text{g}/\text{m}^3$,

256 respectively. For $\text{PM}_{2.5}$, the R^2 values were 0.83 and 0.52, with RMSE values of $16.46 \mu\text{g}/\text{m}^3$ and $28.11 \mu\text{g}/\text{m}^3$, respectively. The DOET model is relatively robust based on sample and spatial validation results.



258
259 **Figure 2. Spatial distribution of PM_{10} and $\text{PM}_{2.5}$ and cross validation results of the DOET model. The dashed**
260 **lines represent the 1:1 line, while the solid lines show the fitted line between observed and estimated values.**

261 By inputting TOAR, meteorological elements and geographical information into the optimally
262 parameterized DOET model, a pollutant estimation dataset for eastern China was generated for the period
263 September 2015 to August 2023. Due to the incomplete spatial coverage of TOAR data in different
264 months and hours (Song et al., 2024), the study first calculated monthly averages, which were then used
265 to derive annual averages. This step helps to minimize errors due to insufficient spatial coverage of the
266 samples (Ding et al., 2024). As shown in Figures 2A and 2B, the Beijing-Tianjin-Hebei region, the
267 Sichuan Basin, the Guanzhong region, and central China are hotspots for PM_{10} and $\text{PM}_{2.5}$ pollution (Wei
268 et al., 2021a), with concentrations reaching up to $100 \mu\text{g}/\text{m}^3$ for PM_{10} and $60 \mu\text{g}/\text{m}^3$ for $\text{PM}_{2.5}$. In addition,
269 the Inner Mongolia region and northern Gansu, which are frequently affected by dust storms, are also
270 characterized by high PM_{10} concentrations (Li et al., 2012). Overall, the PM_{10} and $\text{PM}_{2.5}$ concentrations

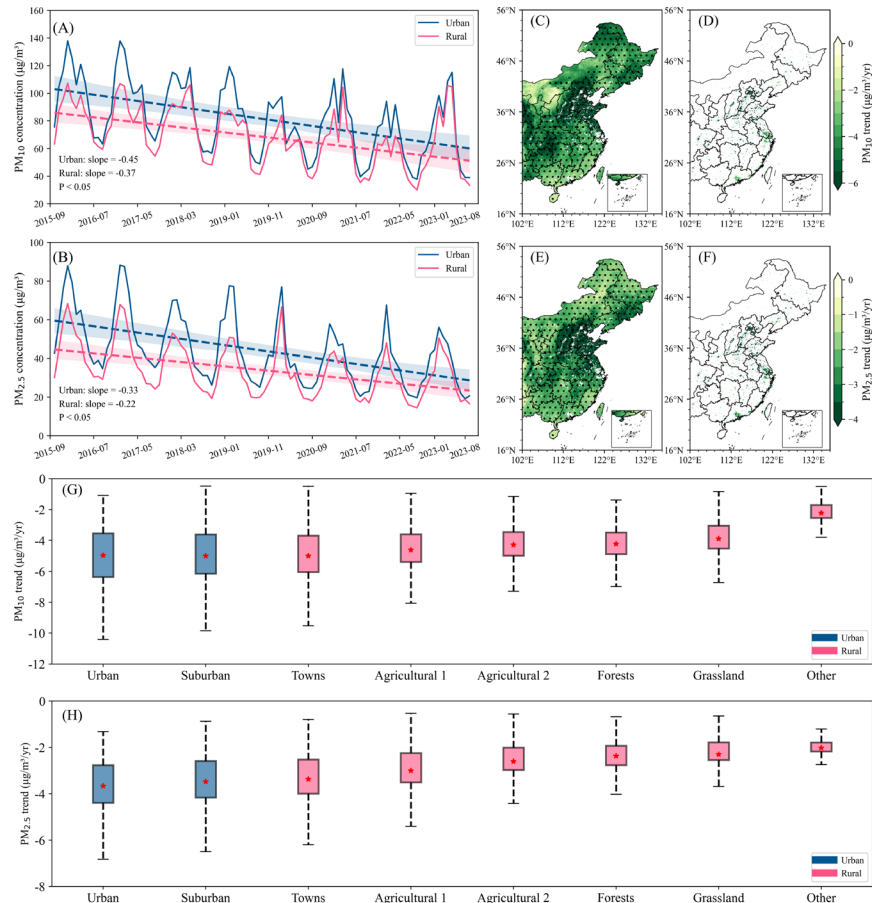
271 generated by the DOET model accurately reflect the spatial distribution characteristics of PM in eastern
272 China, and the estimation results are consistent with those of previous studies (Yang et al., 2023; Chen
273 et al., 2022b; Song et al., 2022a).

274 **3.2 Urban-rural differences in PM pollution trends in recent years**

275 The spatial distribution characteristics of PM_{10} and $PM_{2.5}$ trends from 2015 to 2023 were analysed,
276 and the results (Figures 3C-F) show a remarkable improvement of PM pollution in eastern China, as
277 indicated by a significant decreasing trend in PM concentrations. The average decrease for PM_{10} was -
278 $4.02 \pm 1.29 \mu\text{g}/\text{m}^3/\text{yr}$, while for $PM_{2.5}$, it was $-2.41 \pm 0.91 \mu\text{g}/\text{m}^3/\text{yr}$. However, this widespread decrease in
279 PM concentrations showed considerable spatial heterogeneity between urban and rural areas. The urban
280 and rural decrease trends for PM_{10} were $-4.99 \pm 1.68 \mu\text{g}/\text{m}^3/\text{yr}$ and $-3.98 \pm 1.26 \mu\text{g}/\text{m}^3/\text{yr}$, respectively,
281 while for $PM_{2.5}$, they were $-3.43 \pm 1.10 \mu\text{g}/\text{m}^3/\text{yr}$ and $-2.38 \pm 0.88 \mu\text{g}/\text{m}^3/\text{yr}$, respectively. This suggests
282 that the decrease in PM concentrations in rural areas was close to the regional average in eastern China,
283 while the decrease in urban areas was more pronounced than the overall trend. We supplemented our
284 analysis by examining the relative change trends through benchmark concentration standardization.
285 Initially, the standard deviation of PM concentrations was computed for each grid point to assess spatial
286 variability. Subsequently, the annual mean PM data were used to calculate yearly relative changes
287 normalized against benchmark concentrations. Finally, a comprehensive trend analysis was performed
288 on these standardized values. The results are presented in Figure S2. Consistent with the overall trends
289 in PM concentrations, the relative change rates of $PM_{2.5}$ were quantified as $-38.24 \pm 3.40\%/\text{yr}$ in rural
290 areas and $-40.93 \pm 1.91\%/\text{yr}$ in urban areas. Similarly, PM_{10} exhibited relative change trends of -34.03
291 $\pm 6.55\%/\text{yr}$ (rural) and $-39.07 \pm 2.78\%/\text{yr}$ (urban). These findings demonstrate that, when accounting for
292 region-specific baseline concentrations across different land cover types, urban areas continue to show a
293 more substantial reduction in PM pollution compared to rural areas.

294 From a broader perspective of the changes in particulate matter concentrations in eastern China, the
295 urban decrease trends for PM_{10} and $PM_{2.5}$ were $-0.47 \mu\text{g}/\text{m}^3/\text{month}$ and $-0.33 \mu\text{g}/\text{m}^3/\text{month}$, respectively,
296 while the rural decrease trends were $-0.37 \mu\text{g}/\text{m}^3/\text{month}$ and $-0.22 \mu\text{g}/\text{m}^3/\text{month}$, respectively. These
297 results indicate that the reduction trend in rural areas was slower than in urban areas. By 2023, particulate
298 matter concentrations in urban areas had decreased from about $20 \mu\text{g}/\text{m}^3$ higher than in rural areas to
299 levels almost equal to those in rural areas.

300 Urban and rural areas, categorized by land cover type, comprised eight different categories. The
 301 study assessed their respective roles in PM concentration reduction trends and found that all eight
 302 categories showed declining PM trends. However, the regions with the highest PM reduction trends were
 303 mainly four types: urban core areas, suburbs, towns and agricultural land 1 (high agricultural pressure).
 304 In contrast, the reduction trends were less pronounced in agricultural land 2 (low agricultural pressure),
 305 forests, grassland and other areas.

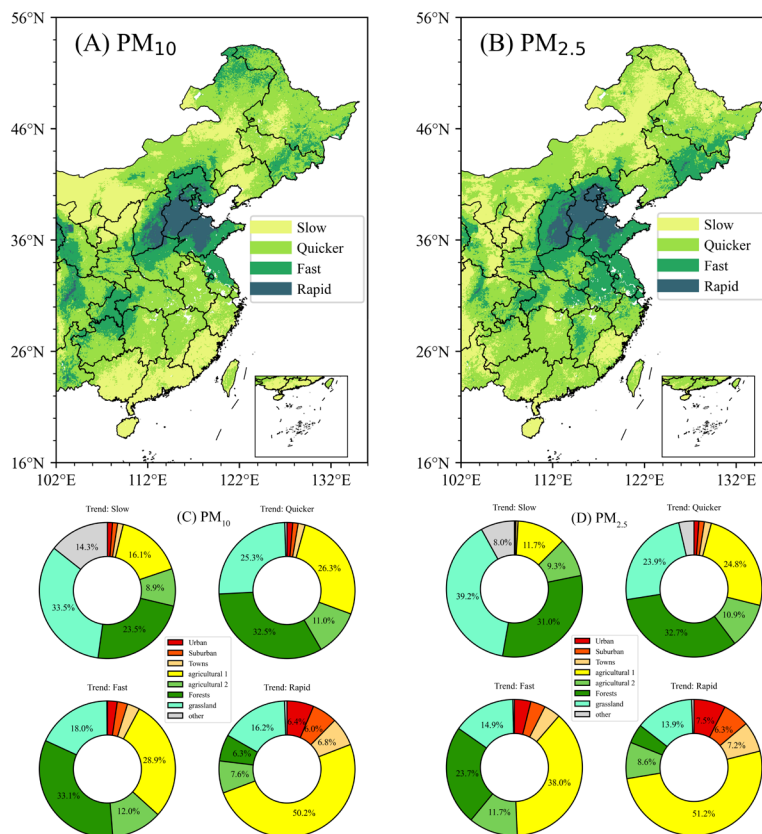


306 **Figure 3. Analysis of PM concentration trends in eastern China from September 2015 to August 2023. Panels**
 307 **A, C, D, and G represent PM₁₀, while panels B, E, F, and H represent PM_{2.5}. In the legends of panels G-H,**
 308 **blue indicates urban areas, and red indicates rural areas. In G and H, the upper part of the box represents**
 309 **the upper quartile of the trend, and the lower part represents the lower quartile of the trend; the dotted line**
 310 **range represents the upper and lower limits of the trend values; the red dot represents the average value of**
 311 **the trend.**

313 The trends in PM₁₀ and PM_{2.5} concentrations were categorized into four levels based on percentiles:
 314 slow decline (grid points with a decline trend below the 25th percentile), moderate decline (grid points
 315 with a decline trend between the 25th and 75th percentiles), rapid decline (grid points with a decline
 316 trend between the 75th and 95th percentiles), and sharp decline (grid points with a decline trend above

317 the 95th percentile). As shown in Figure 4, the regions with the most significant changes in urban and
 318 rural PM trends are mainly concentrated in the Beijing-Tianjin-Hebei region, the Guanzhong region and
 319 Central China.

320 In areas with slow and moderate declines, forests and grasslands accounted for the highest
 321 proportions, ranging from 23.51% to 32.56% and 23.92% to 39.25%, respectively, followed by the
 322 agricultural 1 and agricultural 2, which accounted for about 20%. In regions with rapid decline, the first
 323 type of agricultural land had the highest proportion, ranging from 30 to 40%. Urban core, suburban and
 324 towns had higher proportions in the fast decline regions, accounting for 6.44%, 6.01% and 6.83% of the
 325 PM₁₀ decline trends and 7.52%, 6.34% and 7.21% of the PM_{2.5} decline trends respectively. In particular,
 326 the agricultural 1 had the largest share in the strong decrease regions.



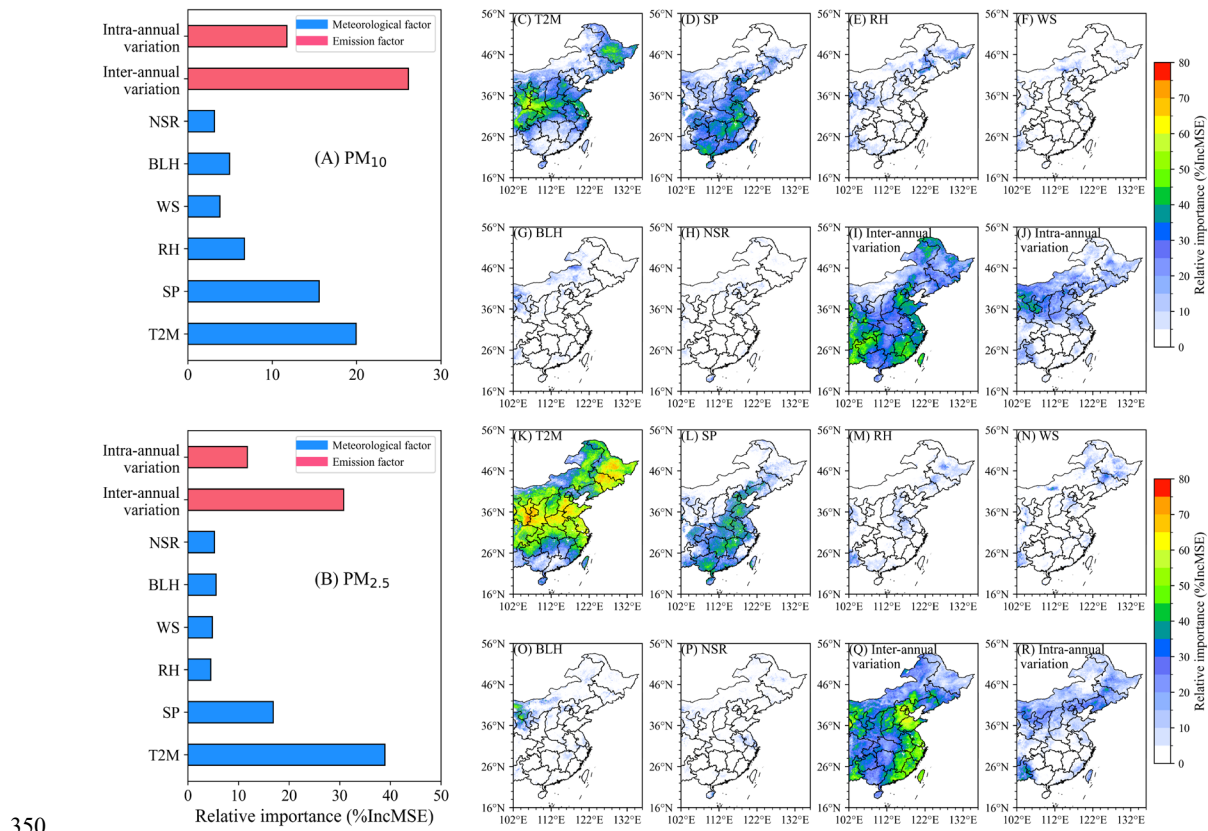
327
 328 **Figure 4. Spatial distribution of particulate matter trend percentiles and pie charts. The individual color**
 329 **scales in the figure represent different areas.**

330 **3.3 Assessing potential driving factors for PM pollution improvement and quantifying their**
 331 **contributions**

332 A DOET model based on monthly PM data was developed to identify the key drivers of urban and
 333 rural particulate matter pollution changes in China. Monthly mean PM₁₀ and PM_{2.5} concentrations were

334 correlated with meteorological factors and two temporal variables (year and month) representing the
 335 effects of meteorological changes and anthropogenic influences, respectively (see Methods for details).
 336 The model was cross-validated using a random training set (70%) and a validation set (30%). As shown
 337 in Figure S3, the DOET model explains more than 60% of the PM₁₀ trends and 80% of the PM_{2.5} trends
 338 in eastern China.

339 The relative importance of each variable in the DOET model was determined using the
 340 permutation_importance library. Inter-annual variability, intra-annual variability, air pressure and
 341 temperature were identified as significant contributors to the improvement of urban and rural PM
 342 pollution in eastern China (relative importance > 10%). Among them, interannual variability was the
 343 most influential factor for PM₁₀ (26.14±13.35%), followed by temperature (19.95±15.06%) (Figure 5A).
 344 In contrast, for PM_{2.5}, interannual variability ranked second (30.79±12.86%), while temperature had a
 345 stronger effect (38.90±17.73%) (Figure 5B). The spatial distribution of the relative importance of the
 346 four main contributing factors, shown in Figures 5C-R, indicates that regions with high relative
 347 importance values overlapped with PM pollution hotspots. Furthermore, as shown in Figure S4, the
 348 driving factors for urban and rural PM pollution improvement differed significantly between land cover
 349 types.

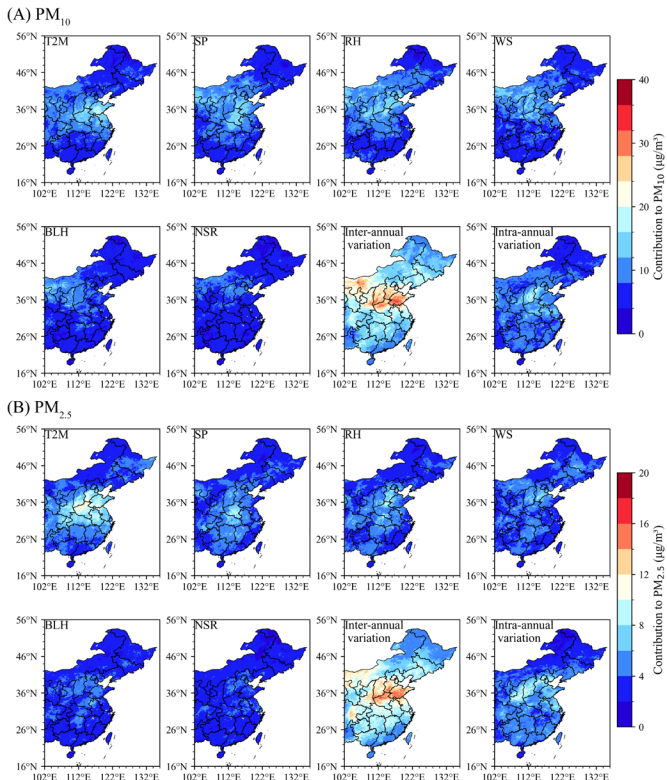


350

351 **Figure 5. Spatial distribution of the relative influence of each variable on PM pollution. In panels (A-B), the**
352 **red variables are related to emissions and the blue variables are related to meteorology.**

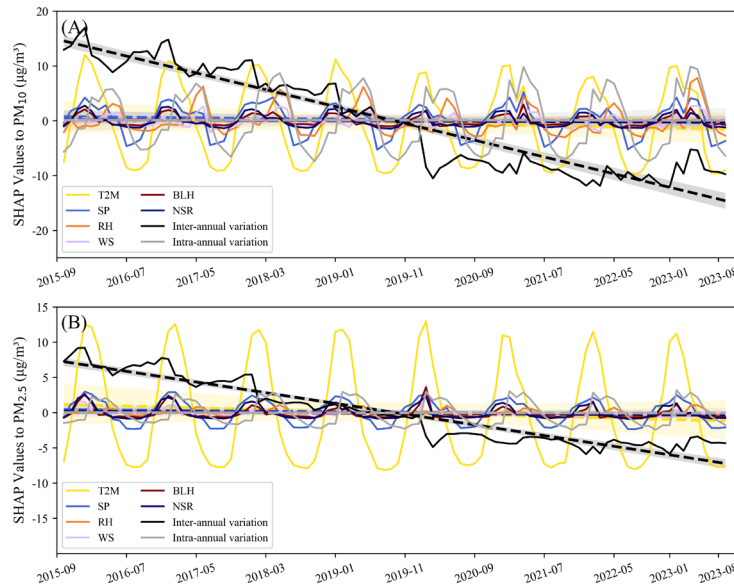
353 The relative contributions of each variable in the DOET model to the PM concentration values were
354 obtained using the permutation_importance library. The results showed that the improvement in urban
355 and rural PM pollution was primarily driven by interannual variation (Figure 5), followed by temperature,
356 which is consistent with the relative importance results in Figure 5. Figure S5-S6 illustrate how variations
357 in the values of the driving factors influence their relative contributions to PM concentrations. In
358 particular, PM concentrations showed a clear inverse relationship with temperature and interannual
359 variations, especially for PM_{2.5}. Relative humidity also showed clear differences in its contribution to
360 PM₁₀ and PM_{2.5}: lower relative humidity was associated with higher PM₁₀ concentrations, whereas higher
361 PM_{2.5} concentrations were associated with higher relative humidity. The scatter plots illustrating the
362 relationships between other variables and their relative contributions to PM are shown in Figures S4-S5.

363 Figure 6 shows the relative contributions of each variable, with the spatial distribution patterns of
364 interannual variations being particularly noteworthy. For PM₁₀, regions such as Guanzhong, North China,
365 and Inner Mongolia were more susceptible to the influence of interannual variations. We hypothesize
366 that the improvement in PM₁₀ pollution be due not only be attributed to anthropogenic emission
367 reductions but also to sandstorm events in recent years, which are important sources of PM₁₀ (Wang et
368 al., 2024c). However, the explanatory power of the model for PM₁₀ trends in these areas remains
369 relatively low, suggesting the need for further investigation into the specific causes. For PM_{2.5}, the impact
370 of interannual variability was observed mainly in the Guanzhong region, North China, and the Sichuan
371 Basin, all of which are key areas for pollution control (Wang et al., 2022a; Yu et al., 2022). Contrary to
372 the relative importance results, the dominant factor driving the improvement in urban and rural PM
373 pollution was the influence of interannual variability (Figure S7), with other variables showing varying
374 effects across different land cover types.



376 **Figure 6. The spatial distribution of the relative contributions of each variable to PM pollution**

377 Finally, the “tree_SHAP” tool was used to decompose the SHAP values of each variable in the
 378 DOET model. By analyzing the positive and negative changes in the SHAP values, the influence of each
 379 variable on the PM pollution improvement - whether positive or negative - was quantified, thus
 380 complementing the assessment of driving factor contributions (Li et al., 2024a). As shown in Figure 7,
 381 the SHAP values show a strong negative correlation between PM concentrations and the contribution of
 382 interannual variability in eastern China. In particular, during the transition from 2019 to 2020, the
 383 contribution of interannual variations to PM concentrations shifted critically from positive to negative.
 384 Interestingly, despite the high relative importance and contribution of some variables, their SHAP values
 385 showed periodic fluctuations, alternating between positive and negative, such as for temperature (with a
 386 negative contribution in summer and a positive one in winter). This suggests that meteorological factors
 387 influence PM concentrations in a periodic manner, while the only factor that consistently contributes to
 388 the improvement of PM pollution is the interannual variation driven by anthropogenic influences. The
 389 Figure S8-S9 show the SHAP values of various variables for PM in urban and rural areas, respectively.
 390 The impact of various variables, including temperature, on PM is primarily evident in urban areas, where
 391 the magnitude of the values and the rate of change are both higher than in rural areas.



392

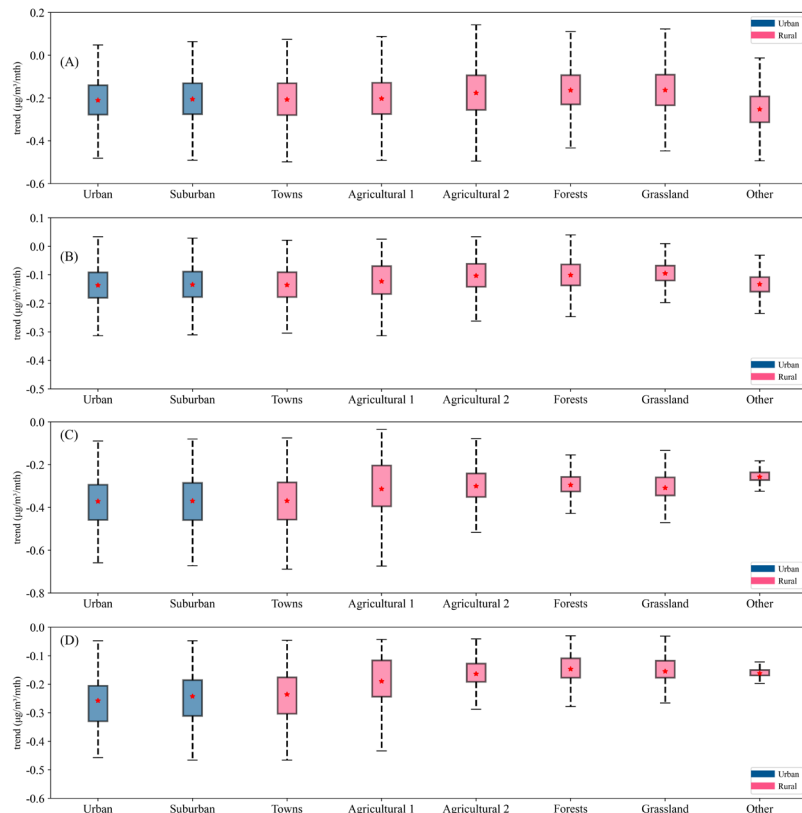
393 **Figure 7. The SHAP values of each variable for PM. The solid line represents the SHAP values, and the dashed
394 line indicates their trend of change.**

395 **3.5 Trends in the contribution of driving factors to PM pollution improvement**

396 To further investigate the influence of potential driving factors on PM concentrations, we conducted
397 a detailed analysis of the trends in the contributions of each variable was performed. As shown in Figures
398 S10-S13, the monthly trends in the relative contributions and SHAP values of each variable were
399 examined, categorized into significant changes ($p < 0.05$) and non-significant changes ($p > 0.05$). For the
400 relative contributions (including PM_{10} and $PM_{2.5}$), with the exception of interannual variations, all other
401 variables showed a decreasing trend, although some regions showed an increasing trend. However, the
402 contribution of interannual variability showed a significant decrease, indicating a reduced capacity of
403 anthropogenic emissions to trigger PM pollution events. This phenomenon is more pronounced for the
404 trends in SHAP values. In particular, only the contribution of interannual variations showed a significant
405 decreasing trend, while the other variables showed non-significant decreasing trends, mainly due to the
406 periodic variations in their contributions, as shown in Figure 7. This shows that the impact of a variable
407 on PM pollution cannot only be assessed on the basis of its relative contribution, but its positive or
408 negative influence on the improvement of PM pollution must also be considered.

409 Given the significant decrease in the contribution of interannual variation, we further compared its
410 trends across different land cover types in urban and rural areas, as this variable plays the most important
411 role in PM pollution improvement. As shown in Figure 8 (A-B), the trends in relative contributions for

412 both PM_{10} and $PM_{2.5}$ did not differ significantly between the eight land cover types, although urban areas
 413 showed the highest rate of decrease. However, the trends in SHAP values shown in Figures 8 (C-D)
 414 revealed that the reduction in the contribution of interannual variation was most pronounced in urban
 415 core areas, suburban areas, and towns. In contrast, the decrease in interannual contributions was more
 416 pronounced in agricultural areas than in urban areas, while other rural areas showed a weaker influence
 417 of interannual variations on PM pollution improvement. These results suggest that the improvement in
 418 PM pollution in urban areas is more closely related to anthropogenic influences, whereas this relationship
 419 is less pronounced in rural areas.



420
 421 **Figure 8. Trends in the relative contribution (A-B) and SHAP values (C-D) of interannual variability of**
 422 **different land cover types. A and C represent the case for PM_{10} , while B and D represent the case for $PM_{2.5}$.**
 423 **In the legend, blue represents urban areas, and red represents rural areas. In Figure 8, the upper part of the**
 424 **box represents the upper quartile of the trend, and the lower part represents the lower quartile of the trend;**
 425 **the dotted line range represents the upper and lower limits of the trend values; the red dot represents the**
 426 **average value of the trend.**

427

428 **4 Discussion and conclusion**

429 Due to the predominant distribution of environmental quality monitoring stations in urban areas

430 (Park et al., 2020), discussions on air pollution patterns between urban and rural regions have been
431 limited (Hammer et al., 2020). In this study, we used a regression-based machine learning DOET
432 algorithm to integrate station-observed PM concentrations, satellite-observed TOAR, meteorological
433 factors, and geographic information data. This approach enabled us to generate long-term, high spatio-
434 temporal resolution datasets of near-surface PM₁₀ and PM_{2.5}, with a spatial resolution of 5 km, an hourly
435 temporal resolution, and coverage across the entire eastern China region. Using the generated PM data
436 in conjunction with a constructed urban-rural land type framework, we successfully captured the broad
437 trends and patterns of PM₁₀ and PM_{2.5} concentration changes from urban and suburban areas to different
438 types of rural regions.

439 Based on the estimated dataset and interpretable parameters, the study identified significant large-
440 scale improvements in PM pollution in eastern China from 2015 to 2023, indicating notable
441 achievements from the implementation of clean air measures. The study noted that the second phase of
442 the clean air action plan, implemented from 2018 to 2020, also produced positive results, following the
443 success of the first phase from 2013 to 2017 (Geng et al., 2024). Our results show that under the urban-
444 rural framework, PM reductions are generally higher in urban areas than in rural areas. However, the
445 highly polluted agricultural areas in rural regions also showed significant improvements in PM pollution.
446 In fact, during air pollution prevention and control efforts, China's main emission reduction measures
447 focused on coal consumption and energy-intensive industries such as steel and cement, and these
448 measures were often effective in urban areas (Yun et al., 2020; Huang et al., 2014b; Wang et al., 2013).
449 This does not mean that rural areas have been neglected, as evidenced by reductions in biomass burning
450 (Shen et al., 2019). The finding that interannual variability is the main driver of PM pollution
451 improvement is consistent with these facts. It is worth noting that the rate of PM concentration decline
452 is faster in urban areas than in rural areas, bringing the concentration levels of the two areas closer
453 together. Given the more pronounced decrease in the contribution of inter-annual variations in urban
454 areas, future efforts to prevent and control air pollution should maintain the current intensity or balance
455 investments between urban and rural areas.

456 Our results indicate that meteorological factors with distinct seasonal variations, such as
457 temperature, boundary layer height, and relative humidity, have a cyclical influence on PM pollution.
458 For example, summer weather conditions, such as abundant precipitation, high relative humidity and

459 abundant water vapour favour PM dispersion, while winter weather conditions are less conducive to
460 pollutant dispersion and spring is often characterised by frequent dust events. Therefore, due to their
461 periodic positive and negative contributions and variability, meteorological conditions do not provide
462 stable improvements in PM pollution. Moreover, the contribution of meteorological conditions to PM
463 concentrations does not show a significant trend. Thus, given the high contribution of inter-annual
464 variability to the improvement of PM pollution, the impact of meteorological conditions on the inter-
465 annual variability of PM pollution in China should not be overemphasised.

466 Although this study evaluated the patterns of PM pollution improvement and its driving factors in
467 urban and rural areas of eastern China, the contribution of interannual variations driven by anthropogenic
468 influences was represented by a time variable in our analysis. In the future, key factors driving changes
469 in air pollutants, such as energy management, urban traffic management, agricultural nitrogen deposition
470 effects and biomass burning, need to be further incorporated into the attribution analysis to distinguish
471 and quantify the contributions of different anthropogenic emission reduction measures to PM pollution
472 improvement. Given the different drivers of PM pollution improvement in urban and rural areas, it is
473 essential to implement tailored strategies in both regions to achieve more effective and comprehensive
474 air pollution prevention and control measures in the future.

475 **Data availability**

476 The hourly ground station observations of near-surface PM₁₀ and PM_{2.5} concentrations are obtained from
477 the China National Environmental Monitoring Center (CNEMC), which can be accessed on its official
478 website (<http://www.cnemc.cn/en/>). Himawari-8 TOAR data provided by the Japan Meteorological
479 Agency, download from: <http://www.eorc.jaxa.jp/ptrec/index.html>. Meteorological variables were
480 derived from the reanalysis data set provided by the European Centre for Medium-Range Weather
481 Forecasts (ECMWF) (<https://cds.climate.copernicus.eu/cdsapp#!/search?type=dataset>). MODIS Land
482 use/cover change (LUCC) product can be downloaded from
483 <https://doi.org/10.5067/MODIS/MCD12C1.061>. The 2015 UN-adjusted population density data (RK)
484 can be downloaded from <https://doi.org/10.7927/H4PN93PB>. SRTM-3 elevation data jointly measured
485 by NASA and the U.S. Department of Defense's National Imagery and Mapping Agency (NIMA)
486 (HEIGHT) can be downloaded from <https://doi.org/10.5067/MEaSUREs/SRTM/SRTMGL3.003>. The

487 particulate matter data generated in the manuscript can be obtained at the following URL:
488 <https://doi.org/10.5281/zenodo.17090707>.

489 **Code availability**

490 The codes are available from the corresponding author upon request.

491 **Acknowledgements**

492 We would like to express our gratitude to the China National Environmental Monitoring Center,
493 Japan Meteorological Agency, European Centre for Medium-Range Weather Forecasts, and NASA
494 for their datasets. The study supported by Supercomputing Center of Lanzhou University.

495 **Financial support**

496 The work was supported by the Noncommunicable Chronic Diseases-National Science and Technology
497 Major Project (Grant number 2024ZD0531600), the National Natural Science Foundation of China
498 (Grant number 42427803), the Gansu Provincial Science and Technology Plan (Grant number
499 25RCKA024), and the Fundamental Research Funds for the Central Universities (Grant number lzujbky-
500 2023-ey10).

501 **Author contributions**

502 Z.S.: Software, Methodology, Data curation, Writing-Original draft preparation, Formal Analysis,
503 Visualization. B.C.: Conceptualization, Methodology, Writing-Reviewing and Editing, Resources.

504 **Competing interests**

505 The authors declare that they have no conflict of interest.

506 **References**

507 An, Z., Huang, R.-J., Zhang, R., Tie, X., Li, G., Cao, J., Zhou, W., Shi, Z., Han, Y., Gu, Z., and Ji, Y.:
508 Severe haze in northern China: A synergy of anthropogenic emissions and atmospheric processes,
509 Proceedings of the National Academy of Sciences, 116, 8657-8666,
510 <https://doi.org/10.1073/pnas.1900125116>, 2019.
511 Apte, J. S., Marshall, J. D., Cohen, A. J., and Brauer, M.: Addressing Global Mortality from Ambient

- 512 PM2.5, Environmental Science & Technology, 49, 8057-8066, <https://doi.org/10.1021/acs.est.5b01236>,
513 2015.
- 514 Berner, L. T., Massey, R., Jantz, P., Forbes, B. C., Macias-Fauria, M., Myers-Smith, I., Kumpula, T.,
515 Gauthier, G., Andreu-Hayles, L., Gaglioti, B. V., Burns, P., Zetterberg, P., D'Arrigo, R., and Goetz, S. J.:
516 Summer warming explains widespread but not uniform greening in the Arctic tundra biome, Nature
517 Communications, 11, 4621, <https://doi.org/10.1038/s41467-020-18479-5>, 2020.
- 518 Bessho, K., Date, K., Hayashi, M., Ikeda, A., Imai, T., Inoue, H., Kumagai, Y., Miyakawa, T., Murata,
519 H., Ohno, T., Okuyama, A., Oyama, R., Sasaki, Y., Shimazu, Y., Shimoji, K., Sumida, Y., Suzuki, M.,
520 Taniguchi, H., Tsuchiyama, H., Uesawa, D., Yokota, H., and Yoshida, R.: An Introduction to Himawari-
521 8/9—Japan’s New-Generation Geostationary Meteorological Satellites, Journal of the
522 Meteorological Society of Japan. Ser. II, 94, 151-183, <https://doi.org/10.2151/jmsj.2016-009>, 2016.
- 523 Brauer, M., Freedman, G., Frostad, J., van Donkelaar, A., Martin, R. V., Dentener, F., Dingenen, R. v.,
524 Estep, K., Amini, H., Apte, J. S., Balakrishnan, K., Barregard, L., Broday, D., Feigin, V., Ghosh, S.,
525 Hopke, P. K., Knibbs, L. D., Kokubo, Y., Liu, Y., Ma, S., Morawska, L., Sangrador, J. L. T., Shaddick,
526 G., Anderson, H. R., Vos, T., Forouzanfar, M. H., Burnett, R. T., and Cohen, A.: Ambient Air Pollution
527 Exposure Estimation for the Global Burden of Disease 2013, Environmental Science & Technology, 50,
528 79-88, <https://doi.org/10.1021/acs.est.5b03709>, 2016.
- 529 Burnett, R., Chen, H., Szyszkowicz, M., Fann, N., Hubbell, B., Pope, C. A., Apte, J. S., Brauer, M.,
530 Cohen, A., Weichenthal, S., Coggins, J., Di, Q., Brunekreef, B., Frostad, J., Lim, S. S., Kan, H., Walker,
531 K. D., Thurston, G. D., Hayes, R. B., Lim, C. C., Turner, M. C., Jerrett, M., Krewski, D., Gapstur, S. M.,
532 Diver, W. R., Ostro, B., Goldberg, D., Crouse, D. L., Martin, R. V., Peters, P., Pinault, L., Tjepkema, M.,
533 van Donkelaar, A., Villeneuve, P. J., Miller, A. B., Yin, P., Zhou, M., Wang, L., Janssen, N. A. H., Marra,
534 M., Atkinson, R. W., Tsang, H., Quoc Thach, T., Cannon, J. B., Allen, R. T., Hart, J. E., Laden, F.,
535 Cesaroni, G., Forastiere, F., Weinmayr, G., Jaensch, A., Nagel, G., Concin, H., and Spadaro, J. V.: Global
536 estimates of mortality associated with long-term exposure to outdoor fine particulate matter, Proceedings
537 of the National Academy of Sciences, 115, 9592-9597, <https://doi.org/10.1073/pnas.1803222115>, 2018.
- 538 Burnett Richard, T., Pope, C. A., Ezzati, M., Olives, C., Lim Stephen, S., Mehta, S., Shin Hwashin, H.,
539 Singh, G., Hubbell, B., Brauer, M., Anderson, H. R., Smith Kirk, R., Balmes John, R., Bruce Nigel, G.,
540 Kan, H., Laden, F., Prüss-Ustün, A., Turner Michelle, C., Gapstur Susan, M., Diver, W. R., and Cohen,
541 A.: An Integrated Risk Function for Estimating the Global Burden of Disease Attributable to Ambient
542 Fine Particulate Matter Exposure, Environmental Health Perspectives, 122, 397-403,
543 <https://doi.org/10.1289/ehp.1307049>, 2014.
- 544 Cao, B. and Yin, Z.: Future atmospheric circulations benefit ozone pollution control in Beijing-Tianjin-
545 Hebei with global warming, Science of The Total Environment, 743, 140645,
546 <https://doi.org/10.1016/j.scitotenv.2020.140645>, 2020.
- 547 Chen, B., Hu, J., and Wang, Y.: Synergistic observation of FY-4A&4B to estimate CO concentration in
548 China: combining interpretable machine learning to reveal the influencing mechanisms of CO variations,
549 npj Climate and Atmospheric Science, 7, 9, <https://doi.org/10.1038/s41612-023-00559-0>, 2024a.
- 550 Chen, B., Song, Z., Pan, F., and Huang, Y.: Obtaining vertical distribution of PM2.5 from CALIOP data
551 and machine learning algorithms, Science of The Total Environment, 805, 150338,
552 <https://doi.org/10.1016/j.scitotenv.2021.150338>, 2022a.
- 553 Chen, B., Song, Z., Shi, B., and Li, M.: An interpretable deep forest model for estimating hourly PM10
554 concentration in China using Himawari-8 data, Atmospheric Environment, 268, 118827,
555 <https://doi.org/10.1016/j.atmosenv.2021.118827>, 2022b.

- 556 Chen, B., Wang, Y., Huang, J., Zhao, L., Chen, R., Song, Z., and Hu, J.: Estimation of near-surface ozone
557 concentration and analysis of main weather situation in China based on machine learning model and
558 Himawari-8 TOAR data, *Science of The Total Environment*, 864, 160928,
559 <https://doi.org/10.1016/j.scitotenv.2022.160928>, 2023.
- 560 Chen, B., Song, Z., Huang, J., Zhang, P., Hu, X., Zhang, X., Guan, X., Ge, J., and Zhou, X.: Estimation
561 of Atmospheric PM10 Concentration in China Using an Interpretable Deep Learning Model and Top-of-
562 the-Atmosphere Reflectance Data From China's New Generation Geostationary Meteorological Satellite,
563 FY-4A, *Journal of Geophysical Research: Atmospheres*, 127, e2021JD036393,
564 <https://doi.org/10.1029/2021JD036393>, 2022c.
- 565 Chen, C.-C., Wang, Y.-R., Yeh, H.-Y., Lin, T.-H., Huang, C.-S., and Wu, C.-F.: Estimating monthly PM2.5
566 concentrations from satellite remote sensing data, meteorological variables, and land use data using
567 ensemble statistical modeling and a random forest approach, *Environmental Pollution*, 291, 118159,
568 <https://doi.org/10.1016/j.envpol.2021.118159>, 2021.
- 569 Chen, G., Li, S., Knibbs, L. D., Hamm, N. A. S., Cao, W., Li, T., Guo, J., Ren, H., Abramson, M. J., and
570 Guo, Y.: A machine learning method to estimate PM2.5 concentrations across China with remote sensing,
571 meteorological and land use information, *Science of The Total Environment*, 636, 52-60,
572 <https://doi.org/10.1016/j.scitotenv.2018.04.251>, 2018a.
- 573 Chen, J., Yin, J., Zang, L., Zhang, T., and Zhao, M.: Stacking machine learning model for estimating
574 hourly PM2.5 in China based on Himawari 8 aerosol optical depth data, *Science of The Total
575 Environment*, 697, 134021, <https://doi.org/10.1016/j.scitotenv.2019.134021>, 2019a.
- 576 Chen, J., Li, Z., Lv, M., Wang, Y., Wang, W., Zhang, Y., Wang, H., Yan, X., Sun, Y., and Cribb, M.:
577 Aerosol hygroscopic growth, contributing factors, and impact on haze events in a severely polluted
578 region in northern China, *Atmos. Chem. Phys.*, 19, 1327-1342, <https://doi.org/10.5194/acp-19-1327-2019>, 2019b.
- 579 Chen, L., Zhu, J., Liao, H., Yang, Y., and Yue, X.: Meteorological influences on PM2.5 and O3 trends
580 and associated health burden since China's clean air actions, *Science of The Total Environment*, 744,
581 140837, <https://doi.org/10.1016/j.scitotenv.2020.140837>, 2020a.
- 582 Chen, S., Guo, J., Song, L., Li, J., Liu, L., and Cohen, J. B.: Inter-annual variation of the spring haze
583 pollution over the North China Plain: Roles of atmospheric circulation and sea surface temperature,
584 *International Journal of Climatology*, 39, 783-798, <https://doi.org/10.1002/joc.5842>, 2019c.
- 585 Chen, X., Zhang, W., He, J., Zhang, L., Guo, H., Li, J., and Gu, X.: Mapping PM2.5 concentration from
586 the top-of-atmosphere reflectance of Himawari-8 via an ensemble stacking model, *Atmospheric
587 Environment*, 330, 120560, <https://doi.org/10.1016/j.atmosenv.2024.120560>, 2024b.
- 588 Chen, Z., Xie, X., Cai, J., Chen, D., Gao, B., He, B., Cheng, N., and Xu, B.: Understanding
589 meteorological influences on PM2.5 concentrations across China: a temporal and spatial perspective,
590 *Atmos. Chem. Phys.*, 18, 5343-5358, <https://doi.org/10.5194/acp-18-5343-2018>, 2018b.
- 591 Chen, Z., Chen, D., Zhao, C., Kwan, M.-p., Cai, J., Zhuang, Y., Zhao, B., Wang, X., Chen, B., Yang, J.,
592 Li, R., He, B., Gao, B., Wang, K., and Xu, B.: Influence of meteorological conditions on PM2.5
593 concentrations across China: A review of methodology and mechanism, *Environment International*, 139,
594 105558, <https://doi.org/10.1016/j.envint.2020.105558>, 2020b.
- 595 Cheng, J., Tong, D., Zhang, Q., Liu, Y., Lei, Y., Yan, G., Yan, L., Yu, S., Cui, R. Y., Clarke, L., Geng, G.,
596 Zheng, B., Zhang, X., Davis, S. J., and He, K.: Pathways of China's PM2.5 air quality 2015–2060 in the
597 context of carbon neutrality, *National Science Review*, 8, nwab078, <https://doi.org/10.1093/nsr/nwab078>,
598 2021.
- 599

- 600 Cohen, A. J., Brauer, M., Burnett, R., Anderson, H. R., Frostad, J., Estep, K., Balakrishnan, K.,
601 Brunekreef, B., Dandona, L., Dandona, R., Feigin, V., Freedman, G., Hubbell, B., Jobling, A., Kan, H.,
602 Knibbs, L., Liu, Y., Martin, R., Morawska, L., Pope, C. A., Shin, H., Straif, K., Shaddick, G., Thomas,
603 M., van Dingenen, R., van Donkelaar, A., Vos, T., Murray, C. J. L., and Forouzanfar, M. H.: Estimates
604 and 25-year trends of the global burden of disease attributable to ambient air pollution: an analysis of
605 data from the Global Burden of Diseases Study 2015, *The Lancet*, 389, 1907-1918,
606 [https://doi.org/10.1016/S0140-6736\(17\)30505-6](https://doi.org/10.1016/S0140-6736(17)30505-6), 2017.
- 607 Dai, Q., Hou, L., Liu, B., Zhang, Y., Song, C., Shi, Z., Hopke, P. K., and Feng, Y.: Spring Festival and
608 COVID-19 Lockdown: Disentangling PM Sources in Major Chinese Cities, *Geophysical Research
609 Letters*, 48, e2021GL093403, <https://doi.org/10.1029/2021GL093403>, 2021.
- 610 Ding, Y., Li, S., Xing, J., Li, X., Ma, X., Song, G., Teng, M., Yang, J., Dong, J., and Meng, S.: Retrieving
611 hourly seamless PM_{2.5} concentration across China with physically informed spatiotemporal connection,
612 *Remote Sensing of Environment*, 301, 113901, <https://doi.org/10.1016/j.rse.2023.113901>, 2024.
- 613 Geng, G., Xiao, Q., Zheng, Y., Tong, D., Zhang, Y., Zhang, X., Zhang, Q., He, K., and Liu, Y.: Impact of
614 China's Air Pollution Prevention and Control Action Plan on PM_{2.5} chemical composition over eastern
615 China, *Science China Earth Sciences*, 62, 1872-1884, <https://doi.org/10.1007/s11430-018-9353-x>, 2019.
- 616 Geng, G., Liu, Y., Liu, Y., Liu, S., Cheng, J., Yan, L., Wu, N., Hu, H., Tong, D., Zheng, B., Yin, Z., He,
617 K., and Zhang, Q.: Efficacy of China's clean air actions to tackle PM_{2.5} pollution between 2013 and
618 2020, *Nature Geoscience*, 17, 987-994, 10.1038/s41561-024-01540-z, 2024.
- 619 Geng, G., Xiao, Q., Liu, S., Liu, X., Cheng, J., Zheng, Y., Xue, T., Tong, D., Zheng, B., Peng, Y., Huang,
620 X., He, K., and Zhang, Q.: Tracking Air Pollution in China: Near Real-Time PM_{2.5} Retrievals from
621 Multisource Data Fusion, *Environmental Science & Technology*, 55, 12106-12115,
622 10.1021/acs.est.1c01863, 2021.
- 623 Geurts, P., Ernst, D., and Wehenkel, L.: Extremely randomized trees, *Machine Learning*, 63, 3-42,
624 <https://doi.org/10.1007/s10994-006-6226-1>, 2006.
- 625 Grange, S. K. and Carslaw, D. C.: Using meteorological normalisation to detect interventions in air
626 quality time series, *Science of The Total Environment*, 653, 578-588,
627 <https://doi.org/10.1016/j.scitotenv.2018.10.344>, 2019.
- 628 Gui, K., Che, H., Wang, Y., Wang, H., Zhang, L., Zhao, H., Zheng, Y., Sun, T., and Zhang, X.: Satellite-
629 derived PM_{2.5} concentration trends over Eastern China from 1998 to 2016: Relationships to emissions
630 and meteorological parameters, *Environmental Pollution*, 247, 1125-1133,
631 <https://doi.org/10.1016/j.envpol.2019.01.056>, 2019.
- 632 Hammer, M. S., van Donkelaar, A., Li, C., Lyapustin, A., Sayer, A. M., Hsu, N. C., Levy, R. C., Garay,
633 M. J., Kalashnikova, O. V., Kahn, R. A., Brauer, M., Apte, J. S., Henze, D. K., Zhang, L., Zhang, Q.,
634 Ford, B., Pierce, J. R., and Martin, R. V.: Global Estimates and Long-Term Trends of Fine Particulate
635 Matter Concentrations (1998–2018), *Environmental Science & Technology*, 54, 7879-7890,
636 10.1021/acs.est.0c01764, 2020.
- 637 He, J., Gong, S., Yu, Y., Yu, L., Wu, L., Mao, H., Song, C., Zhao, S., Liu, H., Li, X., and Li, R.: Air
638 pollution characteristics and their relation to meteorological conditions during 2014–2015 in major
639 Chinese cities, *Environmental Pollution*, 223, 484-496, <https://doi.org/10.1016/j.envpol.2017.01.050>,
640 2017.
- 641 He, Q., Cao, J., Saide, P. E., Ye, T., and Wang, W.: Unraveling the Influence of Satellite-Observed Land
642 Surface Temperature on High-Resolution Mapping of Ground-Level Ozone Using Interpretable Machine
643 Learning, *Environmental Science & Technology*, 58, 15938-15948,

644 <https://doi.org/10.1021/acs.est.4c02926>, 2024.

645 Hersbach, H., Bell, B., Berrisford, P., Hirahara, S., Horányi, A., Muñoz-Sabater, J., Nicolas, J., Peubey, C., Radu, R., Schepers, D., Simmons, A., Soci, C., Abdalla, S., Abellan, X., Balsamo, G., Bechtold, P., Biavati, G., Bidlot, J., Bonavita, M., De Chiara, G., Dahlgren, P., Dee, D., Diamantakis, M., Dragani, R., Flemming, J., Forbes, R., Fuentes, M., Geer, A., Haimberger, L., Healy, S., Hogan, R. J., Hólm, E., Janisková, M., Keeley, S., Laloyaux, P., Lopez, P., Lupu, C., Radnoti, G., de Rosnay, P., Rozum, I., Vamborg, F., Villaume, S., and Thépaut, J.-N.: The ERA5 global reanalysis, Quarterly Journal of the Royal Meteorological Society, 146, 1999-2049, <https://doi.org/10.1002/qj.3803>, 2020.

652 Hou, L., Dai, Q., Song, C., Liu, B., Guo, F., Dai, T., Li, L., Liu, B., Bi, X., Zhang, Y., and Feng, Y.: Revealing Drivers of Haze Pollution by Explainable Machine Learning, Environmental Science & Technology Letters, 9, 112-119, <https://doi.org/10.1021/acs.estlett.1c00865>, 2022.

655 Hu, Y., Zeng, C., Li, T., and Shen, H.: Performance comparison of Fengyun-4A and Himawari-8 in PM2.5 estimation in China, Atmospheric Environment, 271, 118898, <https://doi.org/10.1016/j.atmosenv.2021.118898>, 2022.

658 Hua, J., Zhang, Y., de Foy, B., Mei, X., Shang, J., and Feng, C.: Competing PM2.5 and NO₂ holiday effects in the Beijing area vary locally due to differences in residential coal burning and traffic patterns, Science of The Total Environment, 750, 141575, <https://doi.org/10.1016/j.scitotenv.2020.141575>, 2021.

661 Huang, C., Hu, J., Xue, T., Xu, H., and Wang, M.: High-Resolution Spatiotemporal Modeling for Ambient PM2.5 Exposure Assessment in China from 2013 to 2019, Environmental Science & Technology, 55, 2152-2162, 10.1021/acs.est.0c05815, 2021.

664 Huang, R.-J., Zhang, Y., Bozzetti, C., Ho, K.-F., Cao, J.-J., Han, Y., Daellenbach, K. R., Slowik, J. G., Platt, S. M., Canonaco, F., Zotter, P., Wolf, R., Pieber, S. M., Bruns, E. A., Crippa, M., Ciarelli, G., Piazzalunga, A., Schwikowski, M., Abbaszade, G., Schnelle-Kreis, J., Zimmermann, R., An, Z., Szidat, S., Baltensperger, U., Haddad, I. E., and Prévôt, A. S. H.: High secondary aerosol contribution to particulate pollution during haze events in China, Nature, 514, 218-222, <https://doi.org/10.1038/nature13774>, 2014a.

670 Huang, Y., Shen, H., Chen, H., Wang, R., Zhang, Y., Su, S., Chen, Y., Lin, N., Zhuo, S., Zhong, Q., Wang, X., Liu, J., Li, B., Liu, W., and Tao, S.: Quantification of Global Primary Emissions of PM2.5, PM10, and TSP from Combustion and Industrial Process Sources, Environmental Science & Technology, 48, 13834-13843, 10.1021/es503696k, 2014b.

674 Li, J., Wang, Z., Zhuang, G., Luo, G., Sun, Y., and Wang, Q.: Mixing of Asian mineral dust with anthropogenic pollutants over East Asia: a model case study of a super-duststorm in March 2010, Atmos. Chem. Phys., 12, 7591-7607, <https://doi.org/10.5194/acp-12-7591-2012>, 2012.

677 Li, W., Wang, C., Wang, H., Chen, J., Yuan, C., Li, T., Wang, W., Shen, H., Huang, Y., Wang, R., Wang, B., Zhang, Y., Chen, H., Chen, Y., Tang, J., Wang, X., Liu, J., Coveney, R. M., and Tao, S.: Distribution of atmospheric particulate matter (PM) in rural field, rural village and urban areas of northern China, Environmental Pollution, 185, 134-140, <https://doi.org/10.1016/j.envpol.2013.10.042>, 2014.

681 Li, X., Ye, C., Lu, K., Xue, C., Li, X., and Zhang, Y.: Accurately Predicting Spatiotemporal Variations of Near-Surface Nitrous Acid (HONO) Based on a Deep Learning Approach, Environmental Science & Technology, 58, 13035-13046, <https://doi.org/10.1021/acs.est.4c02221>, 2024a.

684 Li, Y., Qiao, L., Liu, M., Yang, Y., Yu, F., Yuan, X., Wang, Q., Ma, Q., and Zuo, J.: Access to affordable and clean domestic heating: A critical review on rural clean heating transformation in China's Jing-Jin-Ji and its surrounding areas, Energy and Buildings, 323, 114829, <https://doi.org/10.1016/j.enbuild.2024.114829>, 2024b.

- 688 Liu, J., Weng, F., and Li, Z.: Satellite-based PM2.5 estimation directly from reflectance at the top of the
689 atmosphere using a machine learning algorithm, *Atmospheric Environment*, 208, 113-122,
690 <https://doi.org/10.1016/j.atmosenv.2019.04.002>, 2019.
- 691 Liu, P., Zhang, C., Xue, C., Mu, Y., Liu, J., Zhang, Y., Tian, D., Ye, C., Zhang, H., and Guan, J.: The
692 contribution of residential coal combustion to atmospheric PM2.5 in northern China during winter,
693 *Atmos. Chem. Phys.*, 17, 11503-11520, 10.5194/acp-17-11503-2017, 2017.
- 694 Liu, R., Ma, Z., Gasparrini, A., de la Cruz, A., Bi, J., and Chen, K.: Integrating Augmented In Situ
695 Measurements and a Spatiotemporal Machine Learning Model To Back Extrapolate Historical Particulate
696 Matter Pollution over the United Kingdom: 1980–2019, *Environmental Science & Technology*, 57,
697 21605-21615, <https://doi.org/10.1021/acs.est.3c05424>, 2023.
- 698 Lundberg, S. M. and Lee, S.-I.: A unified approach to interpreting model predictions, *Proceedings of the*
699 *31st International Conference on Neural Information Processing Systems*, Long Beach, California,
700 USA2017.
- 701 Ma, S., Wang, N., Zhang, J., Ye, D., and Wang, L.: Ammonia chemistry and oxidation dynamics as dual
702 driving factors of PM2.5 nitrate pollution: Insights from the spatiotemporal disparities in central China,
703 *Journal of Environmental Management*, 392, 126594, <https://doi.org/10.1016/j.jenvman.2025.126594>,
704 2025.
- 705 Ministry of Ecology and Environment of the People's Republic of China: Ambient air quality standards,
706 <https://www.mee.gov.cn/ywgl/fgbz/bz/bzwb/dqjhzb/dqhjzlbz/201203/W020120410330232398521.pdf>,
707 last access: 22 October 2024, 2012.
- 708 Ministry of Ecology and Environment of the People's Republic of China: Report on the state of the
709 ecology and environment in China,
710 <http://english.mee.gov.cn/Resources/Reports/soc/SOEE2017/201808/P020180801597738742758.pdf>,
711 last access: 22 October 2024, 2017.
- 712 Park, S., Shin, M., Im, J., Song, C. K., Choi, M., Kim, J., Lee, S., Park, R., Kim, J., Lee, D. W., and Kim,
713 S. K.: Estimation of ground-level particulate matter concentrations through the synergistic use of satellite
714 observations and process-based models over South Korea, *Atmos. Chem. Phys.*, 19, 1097-1113,
715 <https://doi.org/10.5194/acp-19-1097-2019>, 2019.
- 716 Park, S., Lee, J., Im, J., Song, C.-K., Choi, M., Kim, J., Lee, S., Park, R., Kim, S.-M., Yoon, J., Lee, D.-
717 W., and Quackenbush, L. J.: Estimation of spatially continuous daytime particulate matter concentrations
718 under all sky conditions through the synergistic use of satellite-based AOD and numerical models,
719 *Science of The Total Environment*, 713, 136516, <https://doi.org/10.1016/j.scitotenv.2020.136516>, 2020.
- 720 Qin, K., Han, X., Li, D., Xu, J., Loyola, D., Xue, Y., Zhou, X., Li, D., Zhang, K., and Yuan, L.: Satellite-
721 based estimation of surface NO₂ concentrations over east-central China: A comparison of POMINO and
722 OMNO2d data, *Atmospheric Environment*, 224, 117322,
723 <https://doi.org/10.1016/j.atmosenv.2020.117322>, 2020.
- 724 Qiu, M., Zigler, C., and Selin, N. E.: Statistical and machine learning methods for evaluating trends in
725 air quality under changing meteorological conditions, *Atmos. Chem. Phys.*, 22, 10551-10566,
726 <https://doi.org/10.5194/acp-22-10551-2022>, 2022.
- 727 Qu, S., Liu, J., Li, B., Zhao, L., Li, X., Zhang, Z., Yuan, M., Niu, Z., and Lin, A.: Unveiling the driver
728 behind China's greening trend: urban vs. rural areas, *Environmental Research Letters*, 18, 084027,
729 10.1088/1748-9326/ace83d, 2023.
- 730 Rodriguez, J. D., Perez, A., and Lozano, J. A.: Sensitivity Analysis of k-Fold Cross Validation in
731 Prediction Error Estimation, *IEEE Transactions on Pattern Analysis and Machine Intelligence*, 32, 569-

- 732 575, <https://doi.org/10.1109/TPAMI.2009.187>, 2010.
- 733 Shen, G., Ru, M., Du, W., Zhu, X., Zhong, Q., Chen, Y., Shen, H., Yun, X., Meng, W., Liu, J., Cheng, H.,
734 Hu, J., Guan, D., and Tao, S.: Impacts of air pollutants from rural Chinese households under the rapid
735 residential energy transition, *Nature Communications*, 10, 3405, 10.1038/s41467-019-11453-w, 2019.
- 736 Shi, S., Chen, R., Wang, P., Zhang, H., Kan, H., and Meng, X.: An Ensemble Machine Learning Model
737 to Enhance Extrapolation Ability of Predicting Coarse Particulate Matter with High Resolutions in China,
738 *Environmental Science & Technology*, 58, 19325-19337, <https://doi.org/10.1021/acs.est.4c08610>, 2024.
- 739 Shi, Z., Song, C., Liu, B., Lu, G., Xu, J., Van Vu, T., Elliott, R. J. R., Li, W., Bloss, W. J., and Harrison,
740 R. M.: Abrupt but smaller than expected changes in surface air quality attributable to COVID-19
741 lockdowns, *Science Advances*, 7, eabd6696, 10.1126/sciadv.abd6696, 2021.
- 742 Sicard, P., Agathokleous, E., Anenberg, S. C., De Marco, A., Paoletti, E., and Calatayud, V.: Trends in
743 urban air pollution over the last two decades: A global perspective, *Science of The Total Environment*,
744 858, 160064, <https://doi.org/10.1016/j.scitotenv.2022.160064>, 2023.
- 745 Song, C., Liu, B., Cheng, K., Cole, M. A., Dai, Q., Elliott, R. J. R., and Shi, Z.: Attribution of Air Quality
746 Benefits to Clean Winter Heating Policies in China: Combining Machine Learning with Causal Inference,
747 *Environmental Science & Technology*, 57, 17707-17717, <https://doi.org/10.1021/acs.est.2c06800>, 2023.
- 748 Song, Z., Chen, B., and Huang, J.: Combining Himawari-8 AOD and deep forest model to obtain city-
749 level distribution of PM2.5 in China, *Environmental Pollution*, 297, 118826,
750 <https://doi.org/10.1016/j.envpol.2022.118826>, 2022a.
- 751 Song, Z., Zhao, L., Ye, Q., Ren, Y., Chen, R., and Chen, B.: The Reconstruction of FY-4A and FY-4B
752 Cloudless Top-of-Atmosphere Radiation and Full-Coverage Particulate Matter Products Reveals the
753 Influence of Meteorological Factors in Pollution Events, <https://doi.org/10.3390/rs16183363>, 2024.
- 754 Song, Z., Chen, B., Zhang, P., Guan, X., Wang, X., Ge, J., Hu, X., Zhang, X., and Wang, Y.: High temporal
755 and spatial resolution PM2.5 dataset acquisition and pollution assessment based on FY-4A TOAR data
756 and deep forest model in China, *Atmospheric Research*, 274, 106199,
757 <https://doi.org/10.1016/j.atmosres.2022.106199>, 2022b.
- 758 Southerland, V. A., Brauer, M., Mohegh, A., Hammer, M. S., van Donkelaar, A., Martin, R. V., Apte, J.
759 S., and Anenberg, S. C.: Global urban temporal trends in fine particulate matter (PM_{2.5}) and attributable
760 health burdens: estimates from global datasets, *The Lancet Planetary Health*, 6, e139-e146,
761 [https://doi.org/10.1016/S2542-5196\(21\)00350-8](https://doi.org/10.1016/S2542-5196(21)00350-8), 2022.
- 762 State Council of the People's Republic of China: Action Plan on Air Pollution Prevention and Control,
763 http://www.gov.cn/zwgk/2013-09/12/content_2486773.htm, last access: 22 October 2024, 2013.
- 764 State Council of the People's Republic of China: Assessment Method of Air Pollution Prevention and
765 Control Action Plan, http://www.gov.cn/zhengce/content/2014-05/27/content_8830.htm, last access:
766 22 October 2024, 2014.
- 767 Vu, T. V., Shi, Z., Cheng, J., Zhang, Q., He, K., Wang, S., and Harrison, R. M.: Assessing the impact of
768 clean air action on air quality trends in Beijing using a machine learning technique, *Atmos. Chem. Phys.*,
769 19, 11303-11314, <https://doi.org/10.5194/acp-19-11303-2019>, 2019.
- 770 Wang, B., Yuan, Q., Yang, Q., Zhu, L., Li, T., and Zhang, L.: Estimate hourly PM_{2.5} concentrations from
771 Himawari-8 TOA reflectance directly using geo-intelligent long short-term memory network,
772 *Environmental Pollution*, 271, 116327, <https://doi.org/10.1016/j.envpol.2020.116327>, 2021.
- 773 Wang, J., Lin, J., Liu, Y., Wu, F., Ni, R., Chen, L., Ren, F., Du, M., Li, Z., Zhang, H., and Liu, Z.: Direct
774 and indirect consumption activities drive distinct urban-rural inequalities in air pollution-related
775 mortality in China, *Science Bulletin*, 69, 544-553, <https://doi.org/10.1016/j.scib.2023.12.023>, 2024a.

- 776 Wang, R., Tao, S., Ciais, P., Shen, H. Z., Huang, Y., Chen, H., Shen, G. F., Wang, B., Li, W., Zhang, Y.
777 Y., Lu, Y., Zhu, D., Chen, Y. C., Liu, X. P., Wang, W. T., Wang, X. L., Liu, W. X., Li, B. G., and Piao, S.
778 L.: High-resolution mapping of combustion processes and implications for CO₂ emissions, Atmos. Chem. Phys., 13, 5189-5203, 10.5194/acp-13-5189-2013, 2013.
779
- 780 Wang, W., Zhao, C., Dong, C., Yu, H., Wang, Y., and Yang, X.: Is the key-treatment-in-key-areas
781 approach in air pollution control policy effective? Evidence from the action plan for air pollution
782 prevention and control in China, Science of The Total Environment, 843, 156850,
783 <https://doi.org/10.1016/j.scitotenv.2022.156850>, 2022a.
- 784 Wang, X., Wang, T., Xu, J., Shen, Z., Yang, Y., Chen, A., Wang, S., Liang, E., and Piao, S.: Enhanced
785 habitat loss of the Himalayan endemic flora driven by warming-forced upslope tree expansion, Nature
786 Ecology & Evolution, 6, 890-899, <https://doi.org/10.1038/s41559-022-01774-3>, 2022b.
- 787 Wang, Y., Hu, Y., Jiang, S., and Zhao, B.: Distinguishing urban-rural difference in Chinese population
788 exposure to ambient air pollutants, Atmospheric Environment, 334, 120704,
789 <https://doi.org/10.1016/j.atmosenv.2024.120704>, 2024b.
- 790 Wang, Y., Yu, H., Li, L., Li, J., Sun, J., Shi, J., and Li, J.: Long-term trend of dust event duration over
791 Northwest China, Science of The Total Environment, 951, 175819,
792 <https://doi.org/10.1016/j.scitotenv.2024.175819>, 2024c.
- 793 Wei, J., Huang, W., Li, Z., Xue, W., Peng, Y., Sun, L., and Cribb, M.: Estimating 1-km-resolution PM2.5
794 concentrations across China using the space-time random forest approach, Remote Sensing of
795 Environment, 231, 111221, <https://doi.org/10.1016/j.rse.2019.111221>, 2019.
- 796 Wei, J., Li, Z., Lyapustin, A., Sun, L., Peng, Y., Xue, W., Su, T., and Cribb, M.: Reconstructing 1-km-
797 resolution high-quality PM2.5 data records from 2000 to 2018 in China: spatiotemporal variations and
798 policy implications, Remote Sensing of Environment, 252, 112136,
799 <https://doi.org/10.1016/j.rse.2020.112136>, 2021a.
- 800 Wei, J., Li, Z., Pinker, R. T., Wang, J., Sun, L., Xue, W., Li, R., and Cribb, M.: Himawari-8-derived
801 diurnal variations in ground-level PM2.5 pollution across China using the fast space-time Light Gradient
802 Boosting Machine (LightGBM), Atmos. Chem. Phys., 21, 7863-7880, 10.5194/acp-21-7863-2021,
803 2021b.
- 804 Wei, J., Li, Z., Xue, W., Sun, L., Fan, T., Liu, L., Su, T., and Cribb, M.: The ChinaHighPM10 dataset:
805 generation, validation, and spatiotemporal variations from 2015 to 2019 across China, Environment
806 International, 146, 106290, <https://doi.org/10.1016/j.envint.2020.106290>, 2021c.
- 807 Wei, J., Li, Z., Lyapustin, A., Wang, J., Dubovik, O., Schwartz, J., Sun, L., Li, C., Liu, S., and Zhu, T.:
808 First close insight into global daily gapless 1 km PM2.5 pollution, variability, and health impact, Nature
809 Communications, 14, 8349, 10.1038/s41467-023-43862-3, 2023.
- 810 Wei, J., Li, Z., Cribb, M., Huang, W., Xue, W., Sun, L., Guo, J., Peng, Y., Li, J., Lyapustin, A., Liu, L.,
811 Wu, H., and Song, Y.: Improved 1 km resolution PM2.5 estimates across China using enhanced space-
812 time extremely randomized trees, Atmos. Chem. Phys., 20, 3273-3289, <https://doi.org/10.5194/acp-20-3273-2020>, 2020.
- 813
- 814 West, J. J., Cohen, A., Dentener, F., Brunekreef, B., Zhu, T., Armstrong, B., Bell, M. L., Brauer, M.,
815 Carmichael, G., Costa, D. L., Dockery, D. W., Kleeman, M., Krzyzanowski, M., Künzli, N., Liouesse, C.,
816 Lung, S.-C. C., Martin, R. V., Pöschl, U., Pope, C. A., III, Roberts, J. M., Russell, A. G., and Wiedinmyer,
817 C.: "What We Breathe Impacts Our Health: Improving Understanding of the Link between Air Pollution
818 and Health", Environmental Science & Technology, 50, 4895-4904,
819 <https://doi.org/10.1021/acs.est.5b03827>, 2016.

- 820 Xiao, Q., Zheng, Y., Geng, G., Chen, C., Huang, X., Che, H., Zhang, X., He, K., and Zhang, Q.:
821 Separating emission and meteorological contributions to long-term PM2.5 trends over eastern China
822 during 2000–2018, *Atmos. Chem. Phys.*, 21, 9475-9496, <https://doi.org/10.5194/acp-21-9475-2021>,
823 2021.
- 824 Xue, T., Liu, J., Zhang, Q., Geng, G., Zheng, Y., Tong, D., Liu, Z., Guan, D., Bo, Y., Zhu, T., He, K., and
825 Hao, J.: Rapid improvement of PM2.5 pollution and associated health benefits in China during 2013–
826 2017, *Science China Earth Sciences*, 62, 1847-1856, <https://doi.org/10.1007/s11430-018-9348-2>, 2019.
- 827 Yang, J., Lin, Z., and Shi, S.: Household air pollution and attributable burden of disease in rural China:
828 A literature review and a modelling study, *Journal of Hazardous Materials*, 470, 134159,
829 <https://doi.org/10.1016/j.jhazmat.2024.134159>, 2024.
- 830 Yang, N., Shi, H., Tang, H., and Yang, X.: Geographical and temporal encoding for improving the
831 estimation of PM2.5 concentrations in China using end-to-end gradient boosting, *Remote Sensing of
832 Environment*, 269, 112828, <https://doi.org/10.1016/j.rse.2021.112828>, 2022.
- 833 Yang, Q., Kim, J., Cho, Y., Lee, W.-J., Lee, D.-W., Yuan, Q., Wang, F., Zhou, C., Zhang, X., Xiao, X.,
834 Guo, M., Guo, Y., Carmichael, G. R., and Gao, M.: A synchronized estimation of hourly surface
835 concentrations of six criteria air pollutants with GEMS data, *npj Climate and Atmospheric Science*, 6,
836 94, <https://doi.org/10.1038/s41612-023-00407-1>, 2023.
- 837 Yin, J., Mao, F., Zang, L., Chen, J., Lu, X., and Hong, J.: Retrieving PM2.5 with high spatio-temporal
838 coverage by TOA reflectance of Himawari-8, *Atmospheric Pollution Research*, 12, 14-20,
839 <https://doi.org/10.1016/j.apr.2021.02.007>, 2021.
- 840 Yin, P., Brauer, M., Cohen, A. J., Wang, H., Li, J., Burnett, R. T., Stanaway, J. D., Causey, K., Larson, S.,
841 Godwin, W., Frostad, J., Marks, A., Wang, L., Zhou, M., and Murray, C. J. L.: The effect of air pollution
842 on deaths, disease burden, and life expectancy across China and its provinces, 1990–2017: an analysis
843 for the Global Burden of Disease Study 2017, *The Lancet Planetary Health*, 4, e386-e398,
844 [https://doi.org/10.1016/S2542-5196\(20\)30161-3](https://doi.org/10.1016/S2542-5196(20)30161-3), 2020.
- 845 Yu, Y., Dai, C., Wei, Y., Ren, H., and Zhou, J.: Air pollution prevention and control action plan
846 substantially reduced PM2.5 concentration in China, *Energy Economics*, 113, 106206,
847 <https://doi.org/10.1016/j.eneco.2022.106206>, 2022.
- 848 Yun, X., Shen, G., Shen, H., Meng, W., Chen, Y., Xu, H., Ren, Y., Zhong, Q., Du, W., Ma, J., Cheng, H.,
849 Wang, X., Liu, J., Wang, X., Li, B., Hu, J., Wan, Y., and Tao, S.: Residential solid fuel emissions
850 contribute significantly to air pollution and associated health impacts in China, *Science Advances*, 6,
851 eaba7621, 10.1126/sciadv.eaba7621, 2020.
- 852 Zhai, S., Jacob, D. J., Wang, X., Shen, L., Li, K., Zhang, Y., Gui, K., Zhao, T., and Liao, H.: Fine
853 particulate matter (PM2.5) trends in China, 2013–2018: separating contributions from anthropogenic
854 emissions and meteorology, *Atmos. Chem. Phys.*, 19, 11031-11041, <https://doi.org/10.5194/acp-19-11031-2019>, 2019.
- 856 Zhang, H., Di, B., Liu, D., Li, J., and Zhan, Y.: Spatiotemporal distributions of ambient SO₂ across China
857 based on satellite retrievals and ground observations: Substantial decrease in human exposure during
858 2013–2016, *Environmental Research*, 179, 108795, <https://doi.org/10.1016/j.envres.2019.108795>, 2019a.
- 859 Zhang, Q., He, K., and Huo, H.: Cleaning China's air, *Nature*, 484, 161-162,
860 <https://doi.org/10.1038/484161a>, 2012.
- 861 Zhang, Q., Shi, R., Singh, V. P., Xu, C.-Y., Yu, H., Fan, K., and Wu, Z.: Droughts across China: Drought
862 factors, prediction and impacts, *Science of The Total Environment*, 803, 150018,
863 <https://doi.org/10.1016/j.scitotenv.2021.150018>, 2022a.

- 864 Zhang, Q., Zheng, Y., Tong, D., Shao, M., Wang, S., Zhang, Y., Xu, X., Wang, J., He, H., Liu, W., Ding,
865 Y., Lei, Y., Li, J., Wang, Z., Zhang, X., Wang, Y., Cheng, J., Liu, Y., Shi, Q., Yan, L., Geng, G., Hong, C.,
866 Li, M., Liu, F., Zheng, B., Cao, J., Ding, A., Gao, J., Fu, Q., Huo, J., Liu, B., Liu, Z., Yang, F., He, K.,
867 and Hao, J.: Drivers of improved PM2.5 air quality in China from 2013 to 2017, Proceedings of the
868 National Academy of Sciences, 116, 24463-24469, <https://doi.org/10.1073/pnas.1907956116>, 2019b.
869 Zhang, X., Brandt, M., Tong, X., Ciais, P., Yue, Y., Xiao, X., Zhang, W., Wang, K., and Fensholt, R.: A
870 large but transient carbon sink from urbanization and rural depopulation in China, *Nature Sustainability*,
871 5, 321-328, <https://doi.org/10.1038/s41893-021-00843-y>, 2022b.
872 Zhao, B., Zheng, H., Wang, S., Smith, K. R., Lu, X., Aunan, K., Gu, Y., Wang, Y., Ding, D., Xing, J., Fu,
873 X., Yang, X., Liou, K.-N., and Hao, J.: Change in household fuels dominates the decrease in PM2.5
874 exposure and premature mortality in China in 2005–2015, *Proceedings of the National Academy of
875 Sciences*, 115, 12401-12406, <https://doi.org/10.1073/pnas.1812955115>, 2018.
876 Zheng, B., Tong, D., Li, M., Liu, F., Hong, C., Geng, G., Li, H., Li, X., Peng, L., Qi, J., Yan, L., Zhang,
877 Y., Zhao, H., Zheng, Y., He, K., and Zhang, Q.: Trends in China's anthropogenic emissions since 2010 as
878 the consequence of clean air actions, *Atmos. Chem. Phys.*, 18, 14095-14111, <https://doi.org/10.5194/acp-18-14095-2018>, 2018.
879 Zheng, H., Kong, S., He, Y., Song, C., Cheng, Y., Yao, L., Chen, N., and Zhu, B.: Enhanced ozone
880 pollution in the summer of 2022 in China: The roles of meteorology and emission variations,
881 *Atmospheric Environment*, 301, 119701, <https://doi.org/10.1016/j.atmosenv.2023.119701>, 2023.
882 Zhong, Q., Ma, J., Shen, G., Shen, H., Zhu, X., Yun, X., Meng, W., Cheng, H., Liu, J., Li, B., Wang, X.,
883 Zeng, E. Y., Guan, D., and Tao, S.: Distinguishing Emission-Associated Ambient Air PM2.5
884 Concentrations and Meteorological Factor-Induced Fluctuations, *Environmental Science & Technology*,
885 52, 10416-10425, <https://doi.org/10.1021/acs.est.8b02685>, 2018.
886 Zhong, Q., Tao, S., Ma, J., Liu, J., Shen, H., Shen, G., Guan, D., Yun, X., Meng, W., Yu, X., Cheng, H.,
887 Zhu, D., Wan, Y., and Hu, J.: PM2.5 reductions in Chinese cities from 2013 to 2019 remain significant
888 despite the inflating effects of meteorological conditions, *One Earth*, 4, 448-458,
889 <https://doi.org/10.1016/j.oneear.2021.02.003>, 2021.
890

891